Resilience of Prefabricated Concrete Frames using Hybrid Steel-Concrete Composite Connections

Xiao-Fang Deng[1], Teng-Fang Dong[1], Feng Fu[2], and Yun-Hao Weng[1*]

[1] College of Civil Engineering and Architecture, Guilin University of Technology, Guilin, China, 541004.

[2] School of Mathematics, Computer Science and Engineering, City, University of London, EC1V0HB, UK.

Abstract:

The progressive collapse resistance of prefabricated concrete frames with hybrid steel-concrete composite connections (HSCC) is rarely studied. To fill the gap, five (one reinforced concrete (RC) and four prefabricated concrete) 1/2 scaled beam-column sub-assemblages were designed and tested. In four prefabricated concrete specimens, different HSCC types, top and seat with web angle (TSWA), end plate (EP), top and seat angle (TSA), and web cleat (WC), were employed. Experimental results demonstrated that the failure patterns of prefabricated concrete frames with HSCC are different from that of the RC frame counterpart. The failure of the prefabricated concrete frames is governed by the shear fracture or thread stripping of the bolts in the connections while that of the RC frame is governed by the fracture of beam longitudinal rebar. Due to brittle failure of the connections in prefabricated concrete frames, both ultimate bearing capacity and deformation capacity of prefabricated concrete frames are smaller than the corresponding RC frame. Among them, the prefabricated concrete frame with the EP connection achieves the greatest first peak load or compressive arch action capacity. However, no catenary action could be developed in this specimen.

Author Keywords: Disproportionate collapse; Hybrid prefabricated concrete frame; Load resisting mechanism; Beam-column sub-assemblage; Experimental results

* Corresponding author, E-mail address: wengyh@st.gxu.edu.cn

1. Introduction

According to the ASCE/SEI-10 [1], disproportionate collapse is defined as "the spread of an initial local failure from element to element eventually leading to the collapse of an entire structure or a disproportionately large part of it." In recent years, with the frequent occurrence of extreme events, such as terrorist attacks, fires, and explosions, the likelihood of disproportionate collapse caused by extreme loads was increasing. The disproportionate collapse of structure usually results in substantial economic and life loss. How to evaluate or enhance the ability of structures to resist disproportionate collapse has attracted increasing attention from engineers and policymakers. Several design guidelines [1-4] were issued successively. The alternative load path (ALP) method was proposed and gradually became the most popular method in design or academic investigations as it was independent of the extreme loading [5]. Based on the ALP method, many studies were conducted in the past decades [6-9]. Structures may lose columns after an accidental event, causing a significant increase in shear force and flexural bending moment of the adjacent structural components. The beams adjacent to the lost columns can't resist such a significant amount of bending moment purely relying on their flexural strength. Therefore, exploring the inherent potential mechanisms is necessary. The inherent mechanisms include catenary action (CA) and compressive arch action (CAA) of the beams, and tensile membrane action (TMA) and compressive membrane action (CMA) of the slabs.

With the development of modular building technologies, prefabricated concrete (PC) structures have been widely used in developed countries. Several studies [10-15] were carried out to investigate the disproportionate collapse resistance of conventional PC structures with dry or wet connections. Moreover, as steel-concrete composite joints offer an efficient method to connect precast columns and beams, various hybrid steel-concrete composite (HSCC) structures were developed. Compared to the conventional connection of prefabricated concrete structures, the use of hybrid steel-concrete composite (HSCC) connections offers advantages of both steel and concrete materials. It is possible to reduce the size of both hybrid precast beams and columns through effective interaction between the two materials. Moreover, the HSCC connections can be connected by using high-strength bolts or welds, which required less on-site work. Thus, the HSCC structure is ideal for PC buildings [16]. In the past decades, the seismic behavior of PC frames with various types of HSCC connections was investigated. Kulkarni et al. [17] and Li et al. [18] conducted experimental and analytical investigations on HSCC connections subjected to quasi-static cyclic loading to reveal their seismic behavior. It was found that the HSCC connections exhibited sufficient ductility under seismic loading. Li et al. [19] tested a new-type of HSCC connection with end plates to investigate its seismic behavior. It was revealed that the HSCC connection performed even better than the conventional RC connection. Zhang et al. [20] developed a new type of HSCC connection using steel fiber concrete. It was found that the proposed HSCC connection had a satisfactory ability to resist seismic loads. In addition, Zhang et al. [21] designed an innovative type of HSCC connection with energy dissipated plates and I-shaped steel connectors. It revealed that the hybrid joints with the energy dissipated plates and steel fiber concrete performed much better.

From the above investigations, it can be seen that the HSCC connection has been proved to be an effective type of connection for PC frames to resist seismic loadings. However, the characteristics of disproportionate collapse are quite different from those of a seismic hazard: such as the loading direction, monotonic or cyclic, the main load resisting components, etc. Moreover, the resilience of PC frames with HSCC connection to resist disproportionate collapse was still unclear due to few available studies. Therefore, to fill this gap, four PC beam-column assemblies with HSCC connections and one counterpart sub-assemblage using normal RC were designed and tested in this study. The difference between PC frames with HSCC connections and RC frame in terms of load resisting mechanisms were quantified and discussed.

2. Experimental program

2.1. Specimen design

To investigate the resilience of PC frames with HSCC connections, five 1/2 scaled beam-column assemblies were fabricated and tested. Among them, four PC beam-column s assemblies were designed with various HSCC connections and the remaining one is a cast-in-place RC sub-assemblage, which was taken as a control specimen for comparison. The prototype frame of the specimen is a 5-story commercial building that is seismically designed by BS 8110-97 [22], following Kulkarni et al. [17]. Both longitudinal and transverse spans of the prototype frame are 6 m. The story height is 4.1 m. It was assumed that a middle column on the ground floor was lost due to extreme loading. The sub-assemblage above the lost column was extracted from the prototype frame for the test. Therefore, all specimens consist of a two-span beam, a short middle column stub, two side columns, and two overhanging beams, as shown in Fig. 1. The height of the side column and the length of the overhanging beam is determined by the position of inflection points. It was assumed that the inflection points were in the middle height of the column and 1/5 span of the beam. The cast-in-place RC specimen was named as RC-Con, and its dimensions and rebar details are illustrated in Fig. 2. As can be seen in the figure, the clear span of the beam is 2750 mm. The cross-section of the beam and column is 150 mm × 250 mm and 250 mm × 250 mm, respectively. In this study, a relatively low reinforcement ratio is used to make the effect of CAA obvious. T10 and T13 are used as longitudinal rebar while R6 is used as transverse rebar. The beam transverse rebar in the potential plastic hinge zone and the remaining zones were R6@70mm and R6@140mm, respectively, to follow the seismic design details. “T” and “R” represent deformed rebar and plain rebar, respectively. Detailed specimen properties of RC-Con were shown in Table 1.

For PC specimens, four different bolted connections were investigated. Based on the connection types, the specimens were named as follows: PC specimen with TSWA connection was named as PC-TSWA, PC specimen with end plate connection was named as PC-EP, PC specimen with top and seat angle connection was named as PC-TSA, and PC specimen with web cleat connection was named as PC-WC. As shown in Fig. 3, except for the beam-column connection, the dimensions and rebar details of the PC specimens are identical to those of the control specimen RC-Con. The detailing of different HSCC connections is shown in Fig. 4 and tabulated in Table 2, and the detailed fabrication process was illustrated in Fig. 5. For PC-TSWA, the PC beam and column were connected by top and seat angles with double web angles. The angles were connected to the PC beams and columns using M10 size bolts. In terms of PC-EP, the PC beam was connected to the PC column by an end plate. The end plate was welded to the PC beam, and six M10 bolts were applied to fasten the end plate to the PC column. Only top and seat angles were used to connect the PC beam and column in PC-TSA, and only double web angles were applied to connect the PC beam and column in PC-WC. It should be noted that the connectors of PC beams and columns were made of I-shaped steels with the section of UB178×101×19 and UC 203×203×46, respectively. The length of I-shaped steel in the PC beam is 125 mm and that in the PC column is 710 mm. The strength grade of the I-shaped steel is S355. The longitudinal rebar of the PC beams and columns are welded to the I-shaped connectors. For PC-TSWA, PC-TSA, and PC-WC, steel angles with a section size of L60×6 mm were used. For PC-EP, the end plates were 160×220×10 mm and were welded to the I-shaped connectors in PC columns.

2.2. *Property of materials*

According to the compressive and tensile splitting cylinder tests, the average compression strength and splitting tensile strength of the concrete are 34 MPa and 3.3 MPa, respectively. The critical properties of rebar and steel angles are listed in Table 3.

2.3. Test setup with instrumentation layout

In this study, a displacement-controlled pushdown loading regime was applied. The test setup and instrumentation layout are displayed in Fig. 6. This setup was commonly used for pushdown tests of disproportionate collapse resilience of structures [23-27]. As mentioned above, the specimens were extracted from the prototype frame at contraflexure points and 1/2 scaled down. Thus, the side column was pin supported with a roller installed horizontally at the top of the side column and overhanging beam end to represent the horizontal restraints from adjacent members. An axial force of $0.2 f_c^{'} A_g$ (where $f_c^{'}$ is the cylinder compressive strength of concrete while A_g is the gross area) was applied on the side column. To assess the bridging capacity of the specimen under the loss of a middle column, a vertical displacement with the rate of 0.2mm/s was applied to the top of the middle column by a jack with a 700 mm stroke (Item 1 in Fig. 6). A specially designed steel assembly (Item 3 in Fig. 6) was installed for preventing the undesired out-of-plane failure.

A series of load cells, displacement transducers, and strain gauges were applied before testing. Load pins (Item 6 in Fig. 6) were applied in the pin supports to measure the reaction forces of pin support. Tensile/compressive both way load cell (Item 5 in Fig. 6) was applied in each horizontal roller to record its horizontal reaction force. During testing, the applied vertical load was measured by a load cell (Item 2 in Fig. 6) installed between the hydraulic jack (Item 1 in Fig. 6) and the reaction frame. Seven displacement transducers (Item 7 and 8 in Fig. 6) were applied along the beam span to record beam deflection shape. In addition, a series of strain gauges were glued on the rebar at special positions before casting, as shown in Figs. 2 and 3.

3. Test results

In the present study, one RC and four PC beam-column assemblies were tested by pushdown loading regime to assess the effects of different HSCC connections on the performance of PC frames to resist disproportionate collapse. The key results of the test were listed in Table 4 and discussed below.

3.1 Global behavior

3.1.1 Specimen RC-Con

Specimen RC-Con is the cast-in-place RC beam-column sub-assemblage. The load-middle joint deflection (MJD) relationship and failure pattern of RC-Con are displayed in Figs. 7 and 8, respectively.

Initially, the first crack formed at the beam near the middle column at the MJD of 12 mm. With the MJD further increasing to 15 mm, the RC-Con reached its first yield load (FYL), which was defined as the vertical load corresponding to the first yield of the beam longitudinal rebar, of 25 kN. The actual moment applied at the beam ends near the middle column was 16 kN·m, which is 64% of the maximum moment resisted at the section. Meanwhile, noticeable cracks were formed near the beam ends. When the MJD reached 73 mm, the first peak load (FPL) of 42 kN was measured, which is 168 % of FYL, indicating that the load capacity is increased by 68 % due to the mobilization of CAA. The ratio of the actual moment applied to the maximum moment resisted at the beam ends near the middle column increased to 97 % at this time. When MJD reached 120 mm, the actual moment applied at the beam ends near the middle column attained its maximum. With a further increase in MJD, the existing cracks became wider, and the load resistance began to decrease due to the concrete crushing. Further increasing MJD to 154 mm, fracture was occurred in the rebar near the middle column, resulting in the load resistance dropping to 28 kN. Meanwhile, the widest cracks appeared at the location of curtailment of the beam longitudinal rebar. When MJD reached 309 mm, rebar fracture was also observed in the curtailment region of the longitudinal rebar, leading to a further decrease in the load resistance. Once MJD exceeds 448 mm, the load resistance enhanced rapidly since the development of CA. Finally, the ultimate load capacity (UL) of 39 kN was recorded at the MJD of 672 mm. As displayed in Fig. 8, rebar fracture appeared in the beam ends near the middle column and cut-off points of the longitudinal rebar. Obvious concrete crushing occurred in the beam ends. Many penetrated cracks were formed along the beams due to tensile axial force developed in the CA stage.

3.1.2 Specimen PC-TSWA

Specimen PC-TSWA is a PC beam-column sub-assemblage with HSCC of TSWA connection. The vertical load-MJD relationship and failure pattern are displayed in Figs. 7 and 9. Similar to RC-Con, at the MJD of 10 mm, crack first formed at the beam ends near the middle column. When MJD obtained 38 mm, the FYL was measured at 25 kN. The ratio of the actual moment applied to the maximum moment resisted at the beam ends near the middle column reached 65 %. Further growing MJD to 132 mm, the specimen reached FPL of 33 kN, which is 132 % of FYL, indicating that the load capacity is increased by 32 % because of the mobilization of CAA. At this time, the ratio of the actual moment applied to the maximum moment resisted at the beam ends near the middle column increased to 99%. Then, with the increase of MJD, the load resistance of the specimen decreased slowly due to concrete crushing occurred. Meanwhile, large openings were observed at the edge of the I-shaped connectors near the middle column. The applied moment reached its maximum at MJD of 149 mm. When MJD reached 152 mm and 166 mm, the beam rebar fractured at the edge of the I-shaped connectors near the middle column. When the MJD exceeded 229 mm, the bolts at the top angle near the side column were sheared off. Then, the bolts at the web angle began to be sheared off at the MJD of 326 mm. The CA began to develop at the MJD of 385 mm. Finally, following the shear fracture of the bolts at the bottom angle near the side column, PC-TSWA reached its UL of 19 kN, which was only 58 % of its FPL. As displayed in Fig. 9, rebar fracture occurred at the edge of the I-shaped connectors near the middle column. The failure at the side connection was controlled by bolt fracture in shear. Concrete crushing was observed in the beam ends near the middle column while concrete shed occurred in the beam ends near the side column. The number of flexural cracks was much less than those in RC-Con.

3.1.3 Specimen PC-EP

PC-EP is a PC beam-column sub-assemblage with HSCC of end plate connection. The vertical load-MJD relationship and failure pattern are shown in Figs. 7 and 10, respectively. Different from RC-Con and PC-TSWA, the first crack of PC-EP occurred at the edge of the I-shaped connectors near the middle column at the MJD of 12 mm. When MJD increased to 18 mm, the specimen reached its FYL of 21 kN. The ratio of the actual moment applied to the maximum moment resisted at the beam ends near the middle column reached 48 %. Further increasing the MJD to 55 mm, the FPL of 35 kN, which is 167 % of FYL, was measured. This indicated that the mobilization of CAA increases the load capacity by 67 %. At this time, the ratio of the actual moment applied to the maximum moment resisted at the beam ends near the middle column increased to 95%. Then, with the increase of MJD, thread stripping of the bolt occurred at the connections near the side column, leading to the decrease in load resistance. When the MJD reached 130 mm, the applied moment reached its maximum. At the MJD of 236 mm, the load resistance dropped to zero due to bottom rebar fracture. Finally, further increasing the MJD, as the side connections failed by thread stripping of all bolts, the beams and side columns were separated completely. Therefore, CA was not triggered and the load resistance held steady, which was only about 1 kN. As displayed in Fig. 10, rebar fracture occurred at the edge of the I-shaped connectors near the middle column. Moreover, the beam lost contact with the side column finally due to thread stripping of the bolts. Concrete crushing occurred at the edge of the I-shaped connectors near the middle column. The flexural cracks were much less than those in RC-Con and PC-TSWA. No penetrated cracks formed along the beam due to no CA mobilized during the test.

3.1.4 Specimen PC-TSA

PC-TSA is a PC beam-column sub-assemblage with HSCC of top and seat angle connection. The vertical load-MJD relationship and failure pattern are shown in Figs. 7 and 11, respectively. Similar to RC-Con and PC-TSWA, the first crack of PC-TSA occurred at the beam with the MJD of 8 mm. As the beam longitudinal rebar did not yield before FPL, no FYL is shown herein. The FPL of 20 kN was obtained at the MJD of 87 mm. The ratio of the actual moment applied to the maximum moment resisted at the beam ends near the middle column was 83% at this time. Then, further increasing MJD, the load resistance decreased slowly due to concrete crushing. When MJD reached 204 mm and 261 mm, the angle bolts fractured in shear, leading to the load resistance dropping to 0 kN rapidly. The maximum moment of the beam ends near the middle column was measured at the MJD of 204 mm.

Then, with the increase of MJD, the load resistance increased again. Finally, when MJD reached 432 mm, PC-TSA failed by the shear damage of the bolts and achieved its UL of 10 kN. As shown in Fig. 11, all connections failed by bolt shear fracture. Concrete crushing and spalling appeared in the beam ends. Similar to PC-EP, no penetrated cracks formed in the middle zones of the beam due to mild CA developed.

3.1.5 Specimen PC-WC

PC-WC is a PC beam-column sub-assemblage with HSCC of web cleat connection. The vertical load-MJD relationship and failure pattern are shown in Figs. 7 and 12. The first crack was measured at beam ends at the MJD of 7 mm. Similar to PC-TSA, there was no FYL because no beam longitudinal rebar yielded before FPL. When MJD reached 109 mm, the specimen obtained its FPL of 19 kN. The applied moment at the beam ends near the middle column was 14 kN·m, which is 77% of the maximum moment. Then, the load resistance started to drop slowly accompanied by the concrete crushing and spalling. After the MJD exceed 230 mm, the bolts began to fracture due to shear force. The maximum moment of the beam ends near the middle column was measured at the MJD of 299 mm. Finally, as all bolts of the connection near the middle column were destroyed completely at the MJD of 436 mm, the specimen reached its UL of 12 kN. As shown in Fig. 12, the failure of connections was caused by the shear fracture of bolts. Concrete spalling occurred at beam ends. Similar to PC-EP, PC-TSA, no penetrated cracks occurred in the middle zones of the beam since less tensile axial force developed in the beams.

3.2 Horizontal reactions

As the specimens' arrangements were all symmetrical, the average value of the horizontal reaction forces obtained at both sides of the specimens was used and discussed. The horizontal reaction force-MJD curves of the specimens are displayed in Fig. 13. The maximum horizontal reaction forces of the specimens were tabulated in Table 4. Negative means compression force while positive represents tension force. As given in Fig. 13(c), no tensile horizontal force was measured in PC-EP, which confirmed the above conclusion that no CA was developed in the beams due to complete tread stripping of the bolts at MJD of 337 mm. Different from PC-EP, both tensile and compressive reaction forces were measured in other specimens. The maximum horizontal compression forces of RC-Con, PC-TSWA, PC-EP, PC-TSA, and PC-WC are -71 kN, -65 kN, -67 kN, -56 kN, and -56 kN. The maximum horizontal tension forces of RC-Con, PC-TSWA, PC-TSA, and PC-WC were 95 kN, 47 kN, 20 kN, and 24 kN. Therefore, the CAA and CA developed in PC frames with HSCC connection were weaker than those in RC-Con. Among the PC specimens, PC-EP achieved a similar compressive reaction force as that of PC-TSWA. PC-TSA and PC-WC achieved similar horizontal reaction forces.

As shown in Fig. 13, for all specimens, in the stage of CAA, the compressive reaction force was primarily from the bottom pin support. In the large deformation stage, the tensile reaction force of RC-Con was mainly provided by the horizontal restraint at overhanging beam. However, for PC specimens, the tensile reaction force was mostly from the top horizontal restraint and bottom pin support. This is because, in the large deformation stage, the development of axial force in beams of PC specimens is hindered due to the shear fracture of bolts. Therefore, for PC specimens, the shear forces of the side columns transferred from the beams are small, resulting in a small lateral deformation of the side column. Thus, a relatively small force is transmitted to the horizontal restraint at the overhanging beam.

3.3 Deformation's shape

The deformation's shape of the beams is monitored by LVDTs along the beam. Fig. 14 displays the deformation's shape of the beams of RC-Con and PC-TSWA at critical status. The dashed straight line represented chord rotation. As specified in DoD [4], it is calculated by the ratio of MJD to the clean beam span. As shown in Fig. 14(a), for RC-Con, the beams kept almost straight before the FPL. With the MJD increasing to 250 mm, the rotation of the beam end near the middle column was greater than that near the side column. In the last stage, the chord rotation overestimates the rotation of the beam end near the side column and underestimates the rotation of the beam end near the middle column. This is because the plastic hinge formed at the curtailment of the beam longitudinal rebar. Different from RC-Con, as displayed in Fig. 14(b), the beams in PC-TSWA kept straight during the whole loading history. At the UL stage, the chord rotation could predict the rotation of the beam end near the side column accurately but overestimated the rotation of the beam end near the middle column due to plastic hinges occurring at the edge of the I-shaped connectors. For PC-TSA and PC-WC, the rotation of the beam ends was consistent with the chord rotation well. For PC-EP, the deformation of the beam was similar to that of PC-TSWA.

3.4 Strain gauge results

The location of strain gauges is shown in Figs. 2 and 3. The bottom longitudinal rebar of RC-Con, PC-TSWA, and PC-EP started to yield at the MJD of 15 mm, 38 mm, and 18 mm. However, no yielding was measured in PC-TSA during the whole test history while yielding strain was only measured at PC-WC until the stage of UL. Figs. 15 to 16 show the strain readings along with longitudinal rebar of PC-TSWA, and PC-EP, respectively. For PC-TSWA, after reaching FPL, the compression strain of the rebar near the middle column began to decrease with the increase of MJD, indicating that the CAA stage was shifted into the CA stage. However, beyond the stage of FPL, the decrease in load resistance of PC-EP was due to bolt thread stripping instead of concrete crushing. Therefore, different from other specimens, the compression strain of the rebar near the middle column of PC-EP continued to increase after the stage of FPL, which can be seen in Fig. 16. In addition, for PC-TSWA, in the large deformation stage (UL or MJD = 500 mm), most of the longitudinal rebar was in tension, which indicates that CA could have developed in these specimens. Conversely, most of the longitudinal rebar strains of PC-EP were very low in the large deformation stage, indicating that no CA was developed, which is consistent with the results of vertical loads and horizontal reactions. The development of the rebar strain of RC-con, PC-TSA, and PC-WC is similar to PC-TSWA.

4. Analytical and discussion

4.1 Effects of HSCC connection types

As shown in Table 4, the FPL of PC-TSWA, PC-EP, PC-TSA, and PC-WC is 79 %, 83 %, 48 %, and 45 % of that of RC-Con, respectively. Thus, the PC frames using the proposed four HSCC connections could not achieve equivalent behavior as cast-in-place RC frames regarding FPL. Moreover, the measured deformation capacity of RC-Con, PC-TSWA, PC-TSA, and PC-WC corresponding to their UL is 672 mm, 413 mm, 236 mm, 432 mm, and 436 mm, respectively. Therefore, the deformation capacity of PC-TSWA, PC-EP, PC-TSA, and PC-WC is 61 %, 35 %, 64 %, and 65 % of that of RC-Con, respectively. Furthermore, the UL of PC-TSWA, PC-EP, PC-TSA, and PC-WC is 49 %, 36 %, 26 %, and 31 % of that of RC-Con, respectively. It should be noted that the UL is defined as the peak load in the re-ascending phase of the load history. Therefore, regarding the deformation capacity and UL, the PC frames with the proposed four HSCC connections still could not be equivalent to the cast-in-place frame. The lower FPL is due to the lower strength of the HSCC connection and weaker CAA. On the other hand, the lower deformation capacity is because the failure patterns of all PC specimens are controlled by shear fracture or thread stripping failure of the bolts, which are brittle failures and thus, reduce the ductility of the specimens. In consideration that the failure patterns of PC specimens may be changed if the greater size bolts or weaker steel plates are designed in HSCC connection. Therefore, more studies are urgently in need to further investigate the robustness of PC frames with HSCC connections to resist disproportionate collapse in the future.

For PC specimens, the FPL of PC-EP is larger than that of PC-TSWA. However, due to thread stripping failure at the MJD of 337 mm, which prevents the development of CA and thus, the deformation capacity and UL of PC-EP is much lower than that of PC-TSWA.

4.2 Dynamic ultimate bearing capacity

It should be noted that disproportionate collapse is generally a dynamic process. Therefore, it is needed to assess their dynamic ultimate bearing capacity. Relied on the quasi-static pushdown load-displacement curve, a capacity curve method [28] was adopted to calculate the dynamic ultimate bearing capacity of the specimens. Previous studies [29] had been confirmed the feasibility of this method. The mathematical equation of the capacity curve method is given in Eq. 1:

$$P_d\left(u_d\right) = \frac{1}{u_d}\int_0^{u_d} P_s\left(u\right) d_u \tag{1}$$

where $P_d\left(u_d\right)$ and $P_s\left(u\right)$ represent the capacity function and the nonlinear static loading estimated at the displacement demand u, respectively.

Fig. 17 compares the dynamic load-MJD curves of the test specimens based on the capacity curve method. As displayed in the figure, the dynamic ultimate bearing capacity of PC-TSWA, PC-EP, PC-TSA, and PC-WC is 71 %, 73 %, 47 %, and 42 % of that of RC-Con, respectively. Thus, the quasi-static pushdown curve is a good alternate method for the disproportionate collapse study. The dynamic load increase factor is defined as the ratio of static ultimate bearing capacity to dynamic load-resisting capacity [27]. Based on the test results and analytical results, the dynamic load increase factors of RC-Con, PC-TSWA, PC-EP, PC-TSA, and PC-WC were 1.11, 1.22, 1.25, 1.11, and 1.19. Among them, the dynamic load increase factor of the PC specimens is greater than that of the RC specimen due to the brittle failure that occurred there.

4.3 Effects of steel angles

As shown in Table 4 and Fig. 7, the FPL of PC-TSWA is 165 % and 174 % of that of PC-TSA and PC-WC, respectively. Therefore, the web angles and top and seat angles increase the FPL by 65 % and 74 %, respectively. For UL, PC-TSWA, PC-TSA, and PC-WC are 19 kN, 10 kN, and 12 kN. The corresponding MJD is 413 mm, 432 mm, and 436 mm. The results show that the additional web angle or top and seat angle has little effect on the deformation capacity. However, the web angle and top and seat angle could increase the UL by 90 % and 58 %, respectively. Analytical results indicated that the web angle and top and seat angle enhanced the dynamic ultimate bearing capacity by 50 % and 69 %.

4.4 De-composition of vertical load resistance

According to the force equilibrium of the deformed beam in Fig. 18, the vertical load resistance at the middle column could be divided into:

$$P = \sum_{j=1}^{2} \left(N_j \sin\theta_j + V_j \cos\theta_j \right) \tag{2}$$

where P= the applied load; N_j and V_j = the axial force and shear force; θ_j =the rotation of the beam section at one of the joint interfaces.

Based on Eq. (2), the contribution of the axial force (related to CA) and shear force (related to flexural action) could be calculated. The de-composition of load resistance is shown in Fig. 19. PC-TSWA, PC-TSA, and PC-WC have a similar response as RC-Con in terms of de-composition of load resistance. Before CA is triggered, the contribution of axial force is negative, and the vertical load was mainly provided by the flexural action. After the fracture of the rebars or bolts, the contribution of flexural action dropped significantly. In the CA stage, the contribution of CA is positive, while the contribution of flexural action kept decreasing. When the bottom rebar or bolts of the connection near the middle column fractured entirely, the contribution of flexural action transferred into negative. For PC-EP, as no CA developed, the vertical load is mainly provided by the flexural action while the contribution of CA is positive during the test.

5. Conclusions

To examine the resilience of PC frames using innovative hybrid steel-concrete composite (HSCC) connections to resist disproportionate collapse, a series of four PC beam-column assemblies with various HSCC connections as well as an RC sub-assemblage were tested in this study. Relied on the experimental and analytical results, the main conclusions were given:

1. The failure pattern of PC frames with HSCC connections is different from RC frames. The failure of PC frames with HSCC connection is mainly controlled by the shear failure or thread stripping of the bolts. However, the failure of the RC frame is normally controlled by the fracture of top

longitudinal rebar at cut-off points or bottom longitudinal rebar at beam ends near the middle column. Moreover, the beams in PC frames with HSCC connections kept straight during the test, which means rotation mainly concentrated into the HSCC connection.

2. RC frame has larger FPL and UL than those of PC frames with HSCC. Together with horizontal reaction force results, considerable CAA and catenary action capacity are only measured in PC-TSWA. Almost no catenary action is mobilized in the remaining PC frames with EP, TSA, or WC connections. Thus, the load resisting mechanism of PC frames with HSCC is highly dependent on the type of HSCC connection and different from that in RC frames.
3. Comparing the results of PC-TSWA, PC-TSA, and PC-WC, the web angles and top and seat angles enhanced the first peak load of PC frames by 65 % and 74 %, respectively. In addition, the additional web angles or top and seat angles have little effect on the deformation capacity, but could increase the UL by 90 % and 58 %.
4. De-composition of the vertical load resistance indicated that the load contribution in PC-TSWA, PC-TSA, PC-WC, and RC-Con is similar. In the small deformation stage, the vertical load mainly comes from flexural action. Nevertheless, the vertical load is mainly from the development of catenary action in the large deformation stage. However, for PC-EP, the vertical load is mainly from the flexural action during the test.

Acknowledgements

The authors gratefully acknowledge the financial support provided by the National Natural Science Foundation of China (No. 52022024) and the Natural Science Foundation of Guangxi (No. 2021GXNSFFA196001). Any opinions, findings, and conclusions expressed in this paper do not necessarily reflect the view of the National Natural Science Foundation of China and the Natural Science Foundation of Guangxi.

References

[1] ASCE/SEI, Minimum design loads for buildings and other structures, ASCE/SEI 7, Reston, VA, 424, 2010.

[2] General Services Administration (GSA), Progressive collapse analysis and design guidelines for new federal office buildings and major modernization projects, Washington, DC, 2003.

[3] European Committee for Standardization (CEN), Eurocode 1: Actions on structures. Part 1-7: General actions-Accidental actions, EN 1991-2-7, Brussels, 2006.

[4] Department of Defense (DoD), Design of buildings to resist progressive collapse, Unified Facilities Criteria (UFC) 4-023-03, Washington, DC, 2013.

[5] B.R. Ellingwood, D.O. Dusenberry, Building design for abnormal loads and progressive collapse, Comput.-Aided Civ. Infrastruct. Eng. 20(3) (2005) 194-205.

[6] F. Sadek, J.A. Main, H.S. Lew, Y.H. Bao, Testing and analysis of steel and concrete beam-column assemblies under a column removal scenario, J. Struct. Eng. 137(9) (2011) 881-892.

[7] H. Choi, J. Kim, Progressive collapse-resisting capacity of RC beam-column sub-assemblage, Mag. Concr. Res. 63(4) (2011) 297-310.

[8] J. Yu, K.H. Tan, Special detailing techniques to improve structural resistance against progressive collapse, J. Struct. Eng. 140(3) (2014) 04013077.

[9] K. Qian, B. Li, J. Ma, Load-carrying mechanism to resist progressive collapse of RC buildings, J. Struct. Eng. 141(2) (2015) 04014107.

[10] S.B. Kang, K.H. Tan, Robustness assessment of exterior precast concrete frames under column removal scenarios, J. Struct. Eng. 142(12) (2016) 04016131.

[11] S.B. Kang, K.H. Tan, Progressive collapse resistance of precast concrete frames with discontinuous reinforcement in the joint, J. Struct. Eng. 143(9) (2017) 04017090.

[12] K. Qian, B. Li, Performance of precast concrete substructures with dry connections to resist progressive collapse, J. Perform. Constr. Facil. 32(2) (2018) 04018005-1-14.

[13] D.C. Feng, G. Wu, Y. Lu, Numerical investigation on the progressive collapse behavior of precast reinforced concrete frame subassemblages, J. Perform. Constr. Facil. 32(3) (2018) 04018027.

[14] Y. Zhou, T. Chen, Y. Pei, H.J. Hwang, X. Hu, W. Yi, L. Deng, Static load test on progressive collapse resistance of fully assembled precast concrete frame structure, Eng. Struct. 200 (2019) 109719.

[15] Y. Zhou, X. Hu, Y. Pei, H.J. Hwang, L. Deng, Dynamic load test on progressive collapse resistance of fully assembled precast concrete frame structures, Eng. Struct. 214 (2020) 110675.

[16] S.C. Park, W.K. Hong, S. Kim, X. Wang, Mathematical model of hybrid precast gravity frames for smart construction and engineering, Math. Probl. Eng. 2014 (2014) 1-14.

[17] S.A. Kulkarni, B. Li, W.K. Yip, Finite element analysis of precast hybrid-steel concrete connections under cyclic loading, Steel Const. 64(2) (2008) 190-201.

[18] B. Li, S.A. Kulkarni, C.L. Leong, Seismic performance of precast hybrid-steel concrete connections, J. Earthq. Eng. 13(5) (2009) 667-689.

[19] S. Li, Q. Li, H. Zhang, H. Jiang, L. Yan, W. Jiang, Experimental study of a fabricated confined concrete beam-to-column connection with end-plates, Constr. Build. Mater. 158 (2018) 208-16.

[20] J. Zhang, C. Ding, X. Rong, H. Yang, K. Wang, B. Zhang, Experimental seismic study of precast hybrid SFC/RC beam-column connections with different connection details, Eng. Struct. 208 (2020) 110295.

[21] J. Zhang, C. Ding, X. Rong, H. Yang, Y. Li, Development and experimental investigation of hybrid precast concrete beam-column joints, Eng. Struct. 219 (2020) 110922.

[22] British Standards Institution (BSI), Structural use of concrete: Part 1: Code of practice for design and construction, BS 8110, Milton Keynes, UK, 1997.

[23] J. Yu, K.H. Tan, Structural behavior of reinforced concrete frames subjected to progressive collapse, ACI Struct. J. 114(1) (2017) 63-74.

[24] K. Qian, S.L. Liang, D.C. Feng, F. Fu, G. Wu, Experimental and numerical investigation on progressive collapse resistance of post-tensioned precast concrete beam-column sub-assemblages, J. Struct. Eng. 146(9) (2020) 04020170.

[25] Y.H. Weng, K. Qian, F. Fu, Q. Fang, Numerical investigation on load redistribution capacity of flat slab substructures to resist progressive collapse, J. Build. Eng. 29 (2020) 101109.

[26] K. Qian, S.Y. Geng, S.L. Liang, F. Fu, J. Yu, Effects of loading regimes on the structural behavior of RC beam-column sub-assemblages against disproportionate collapse, Eng. Struct. 251 (2022) 113470.

[27] K. Qian, S.L. Liang, X.Y. Xiong, F. Fu, Q. Fang, Quasi-static and dynamic behavior of precast concrete frames with high performance dry connections subjected to loss of a penultimate column scenario, Eng. Struct. 205 (2020) 110115.

[28] B.A. Izzuddin, A.G. Vlassis, A.Y. Elahazouli, D.A. Nethercot, Progressive collapse of multi-story buildings due to sudden column loss-Part 1: simplified assessment framework, Eng. Struct. 30(5) (2008) 1308-1318.

[29] K. Qian, B. Li, Research advances in design of structures to resist progressive collapse, J. Perform. Constr. Facil. 29(5) (2015) B4014007.

Table 1-Specimen Properties of Specimen RC-Con

Specimen ID	Span (mm)	Beam section (mm×mm)	Column section (mm×mm)	Position of curtailment (mm)	Longitudinal Reinforcements				
					A-A section		B-B section		C-C section
					Top	Bottom	Top	Bottom	
RC-Con	2750	150×250	250×250	900	2T10 (0.48%)	2T10 (0.48%)	1T13+2T10 (0.88%)	2T10 (0.48%)	8T13

Note: The concrete cover thickness is 15 mm; T10 and T13 represent deformed rebar with a diameter of 10 mm and 13 mm, respectively; Reinforcement ratio in brackets is calculated by A_s=b×h_0, where b=150 mm and h_0=220 mm; the A-A, B-B, and C-C sections are given in Fig. 2.

Table 2-Summary of Beam-Column Joint of Precast Specimens

Test ID	Connections	Beam	Column	End plate /Angle	Bolt
PC-TSWA	Top and seat with web angles	UB178×101×19 S355	UC203×203×46 S355	L60×6	Grade 8.8 M10
PC-EP	end plate	UB178×101×19 S355	UC203×203×46 S355	160×220×10	Grade 8.8 M10
PC-TSA	Top and seat angle	UB178×101×19 S355	UC203×203×46 S355	L60×6	Grade 8.8 M10
PC-WC	Web cleat	UB178×101×19 S355	UC203×203×46 S355	L60×6	Grade 8.8 M10

Table 3-Material Properties

Item	Diameter (mm)	Yield strength (MPa)	Ultimate strength (MPa)	Elongation (%)
R6	6	404	575	22.1
T10	10	483	582	11.5
T13	13	533	604	13.2
Angle	N/A	345	488	31.0

Table 4-Main Results Comparison

Test ID	MJD at FYL (mm)	MJD at FPL (mm)	MJD at UL (mm)	MJD at the start of CA (mm)	FYL (kN)	FPL (kN)	UL (kN)	MHTF (kN)	MHCF (kN)
RC-Con	15	73	672	448	25	42	39	95	-71
PC-TSWA	38	132	413	385	25	33	19	47	-65
PC-EP	18	55	236	N/A	21	35	14	N/A	-67
PC-TSA	N/A	87	432	386	N/A	20	10	20	-56
PC-WC	N/A	109	436	393	N/A	19	12	24	-56

Note: MJD means middle joint displacement; CA represents catenary action; FYL, FPL, and UL represent first yield load, first peak load, and ultimate load, respectively; MHTF means the maximum horizontal tension force while MHCF represents maximum horizontal compression force.

List of Figures

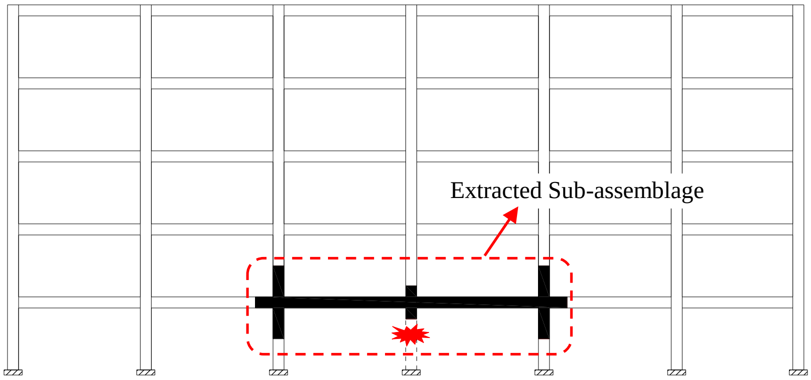

Fig. 1. Elevation view of the prototype building

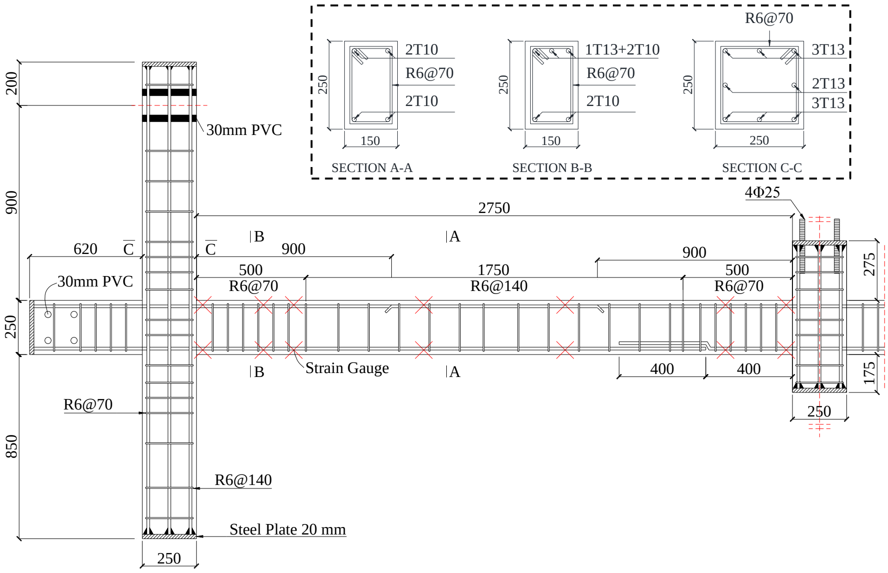

Fig. 2. Dimensions and reinforcement details of Specimen RC-Con

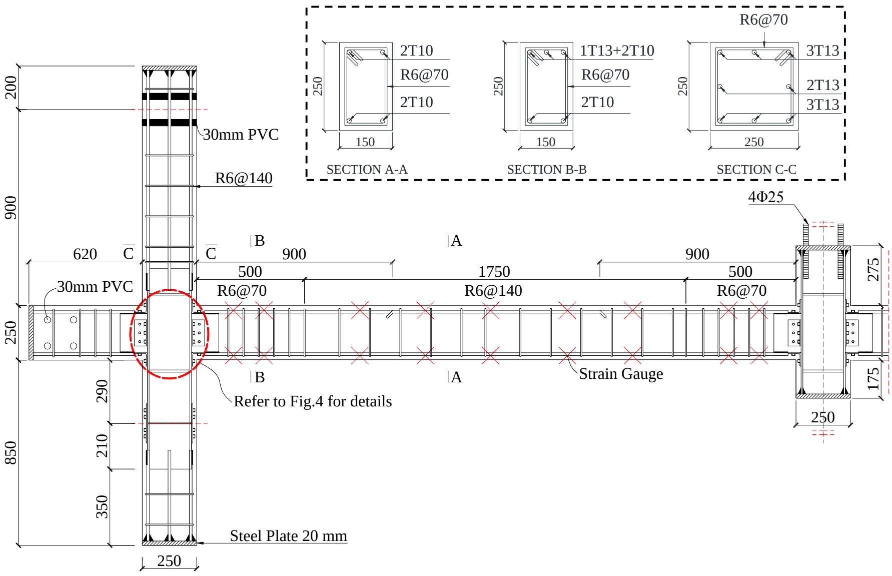

Fig. 3. Dimensions and reinforcement details of precast specimens

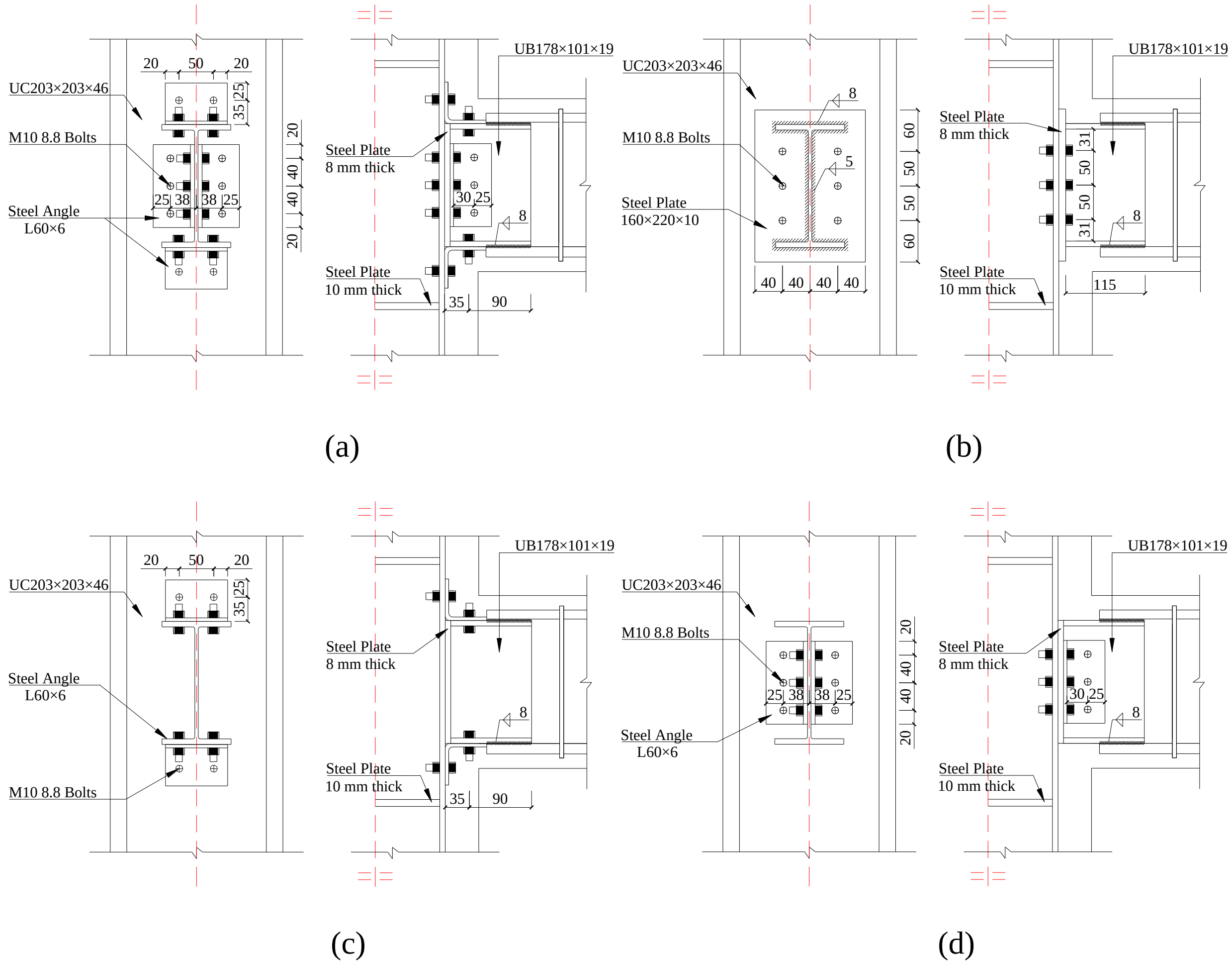

Fig. 4. Connection details: (a) PC-TSWA; (b) PC-EP; (c) PC-TSA; (d) PC-WC

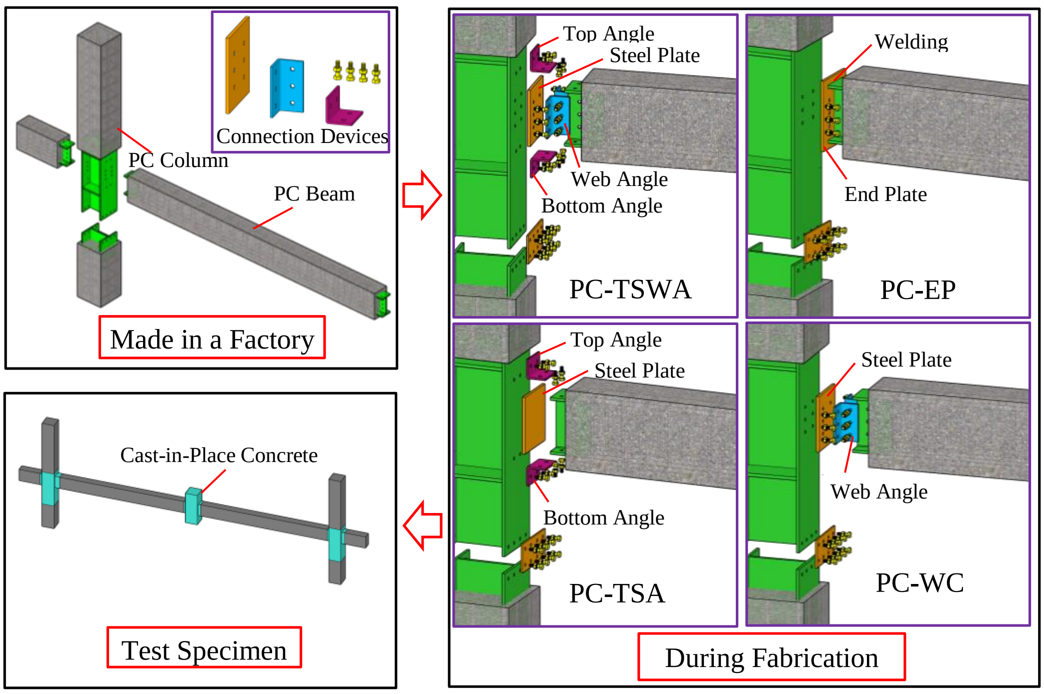

Fig. 5. Fabrication process of the PC specimens

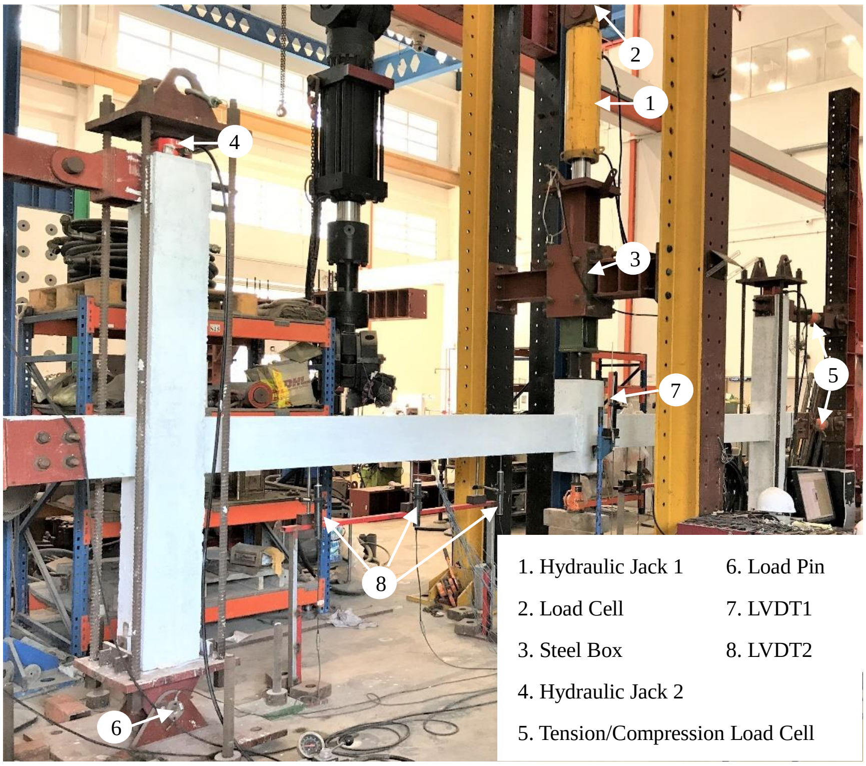

Fig. 6. Test setup

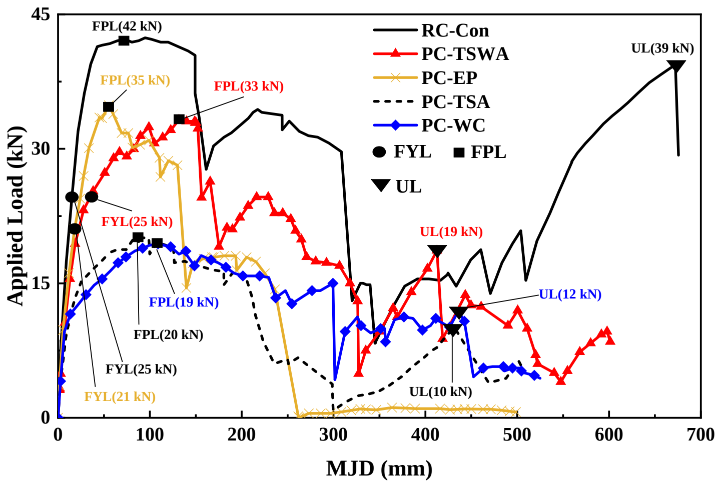

Fig. 7. Vertical load-MJD relationships of specimens

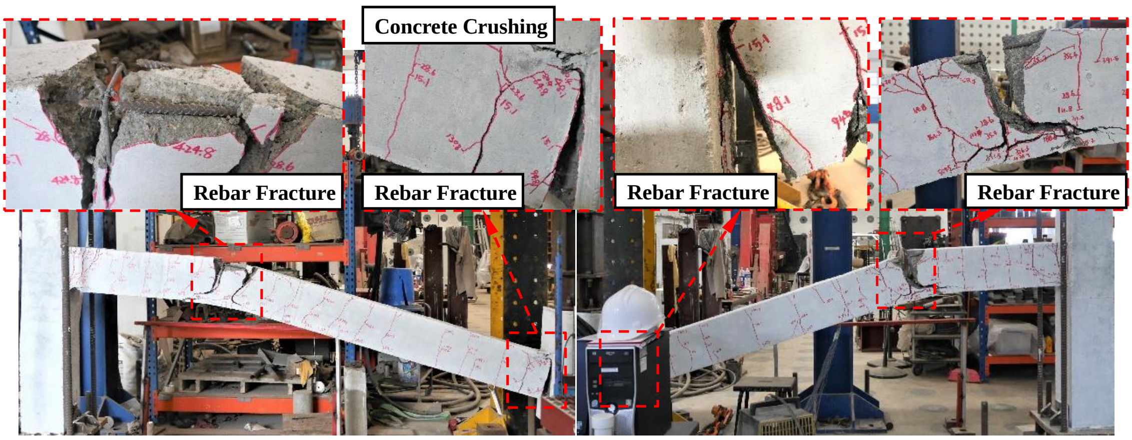

Fig. 8. Failure pattern of RC-Con

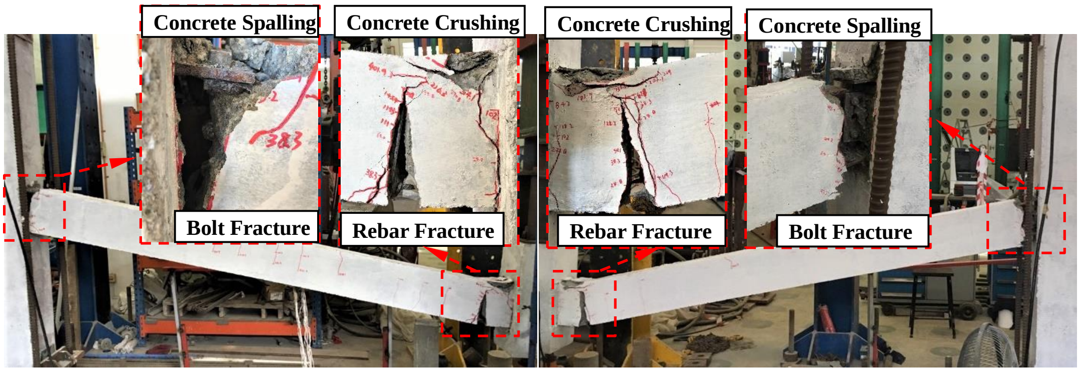

Fig. 9. Failure pattern of PC-TSWA

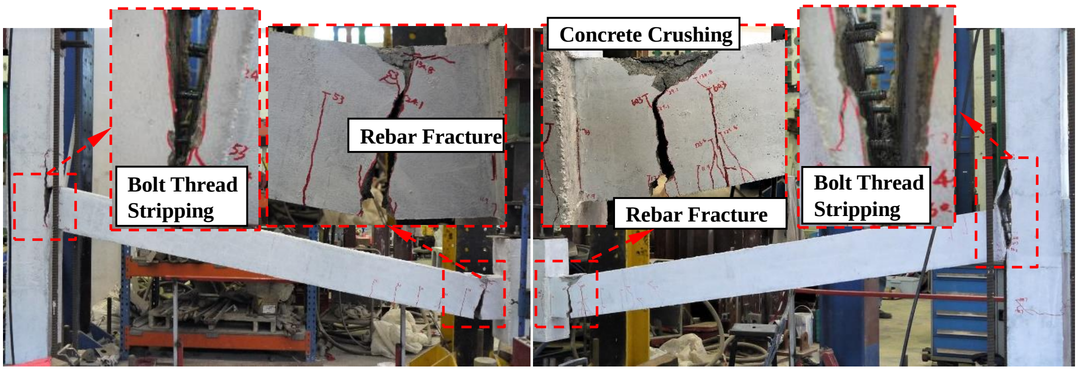

Fig. 10. Failure pattern of PC-EP

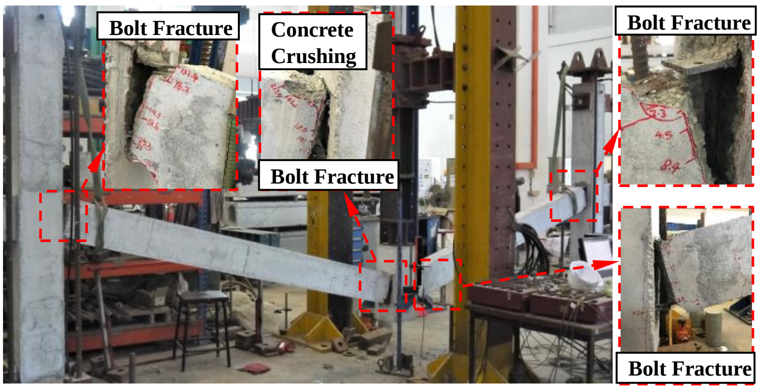

Fig. 11. Failure pattern of PC-TSA

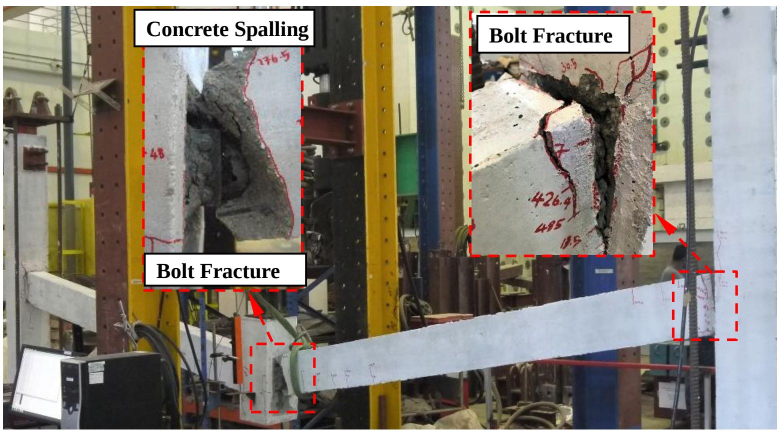

Fig. 12. Failure pattern of PC-WC

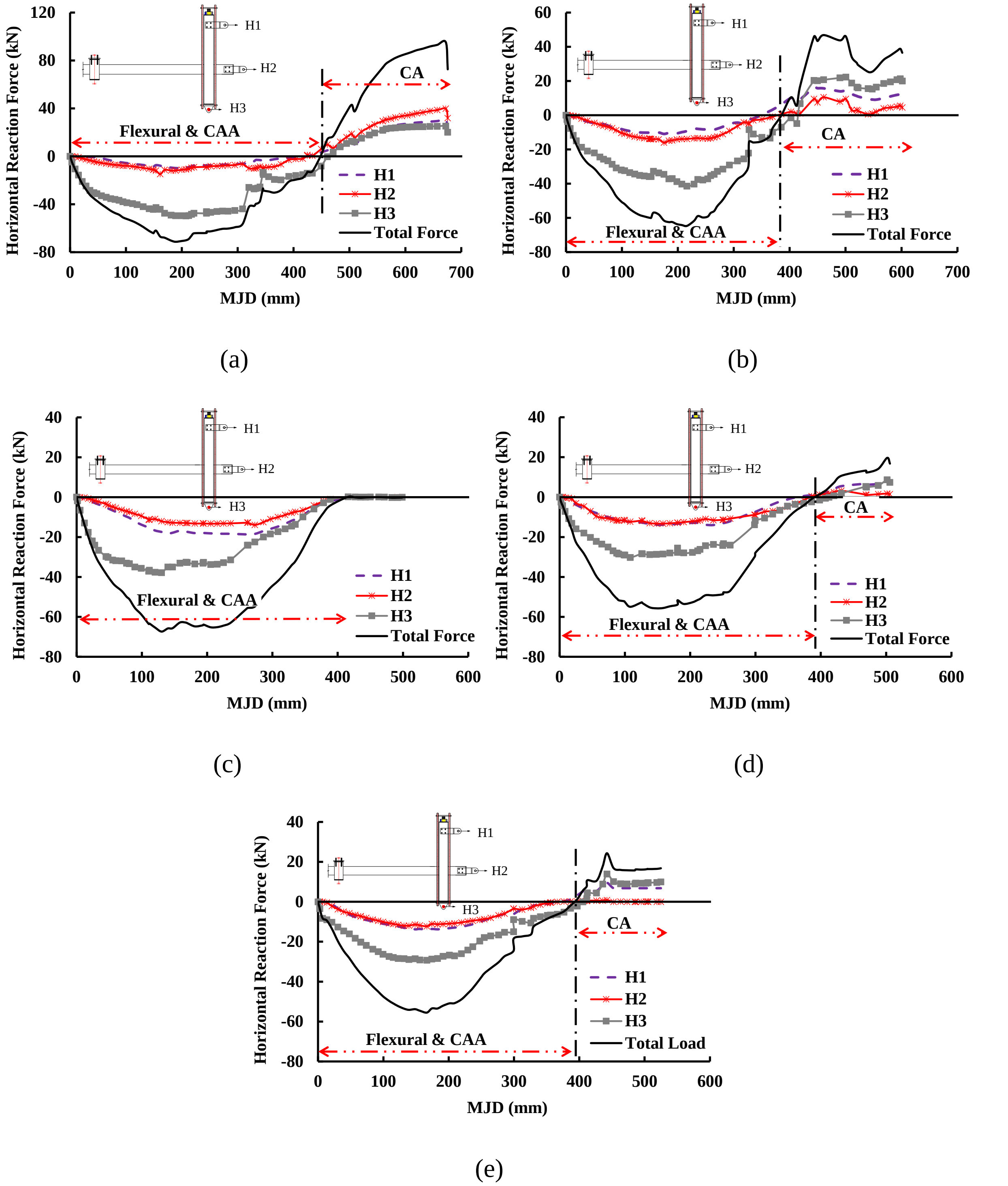

Fig. 13. Horizontal reaction force versus MJD: (a) RC-Con; (b) PC-TSWA; (c) PC-EP; (d) PC-TSA; (e) PC-WC

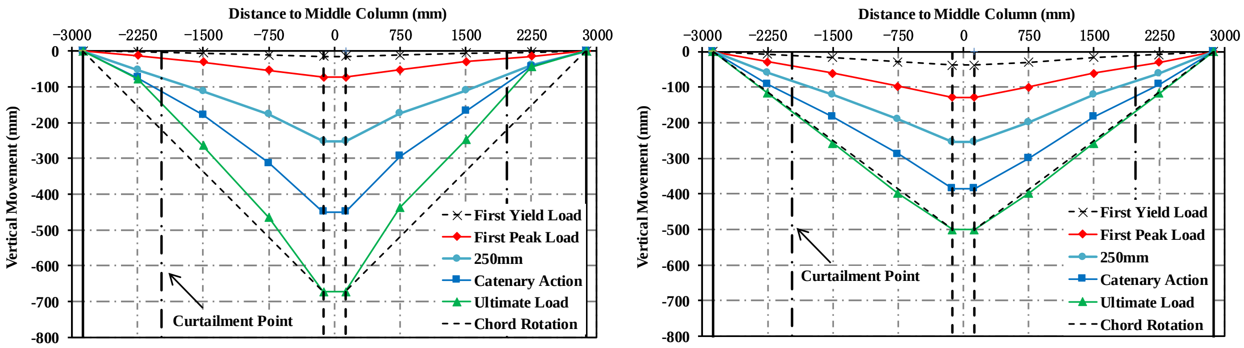

(a) (b)

Fig. 14. Deformation shape of double-span beam: (a) RC-Con; (b) PC-TSWA

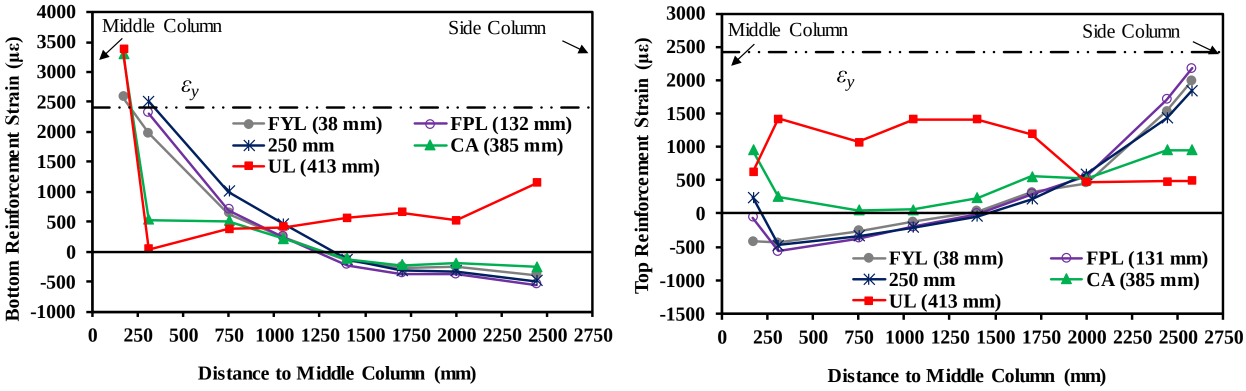

(a) (b)

Fig. 15. Strain distribution along beam rebar of PC-TSWA: (a) bottom rebar; (b) top rebar

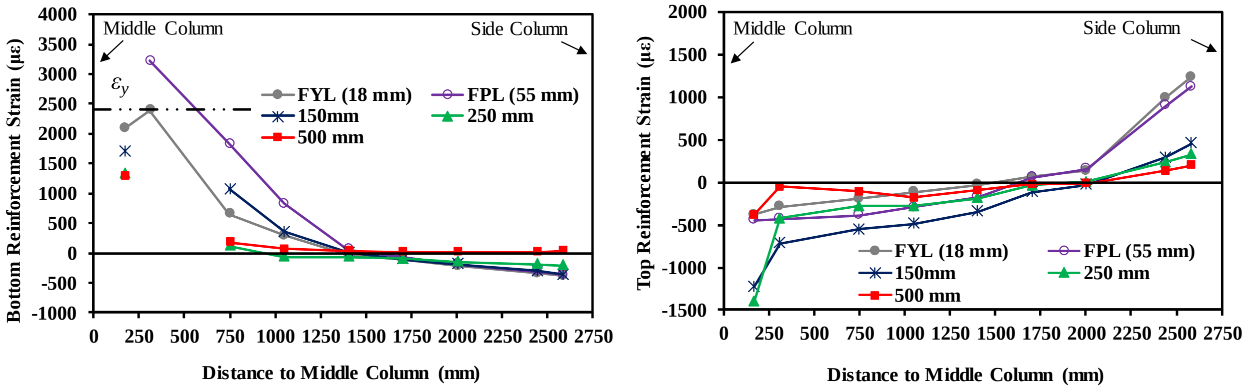

(a) (b)

Fig. 16. Strain distribution along beam rebar of PC-EP: (a) bottom rebar; (b) top rebar

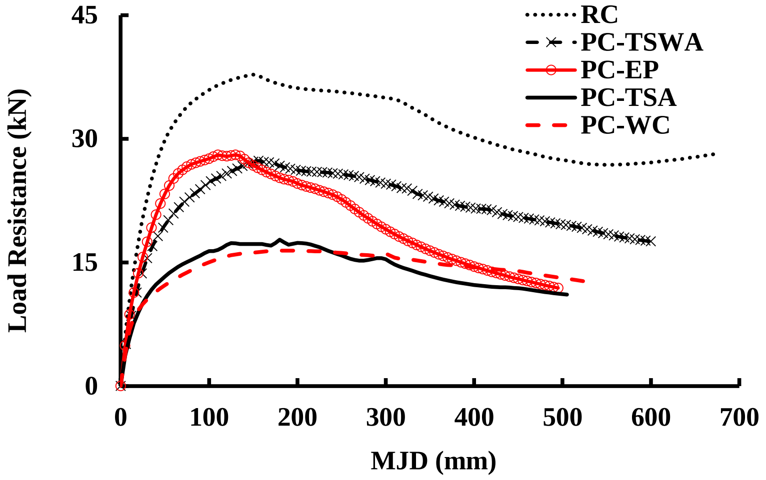

Fig. 17. Dynamic resistance of tested specimens

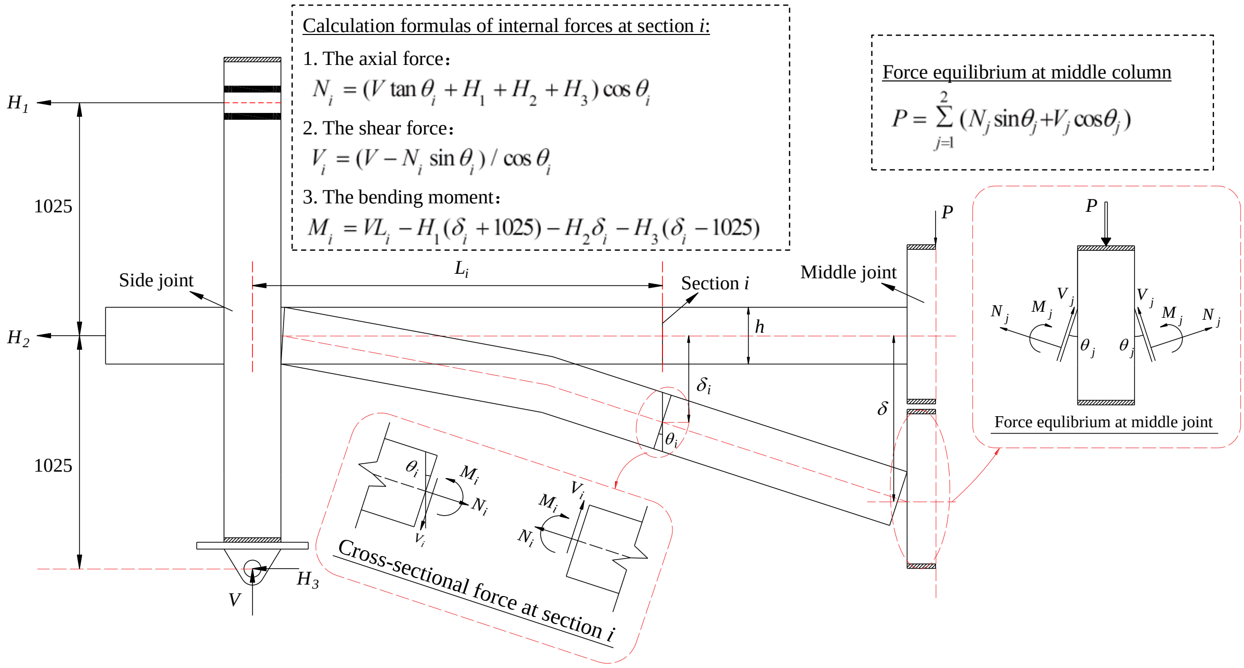

Fig. 18. Calculation of internal forces

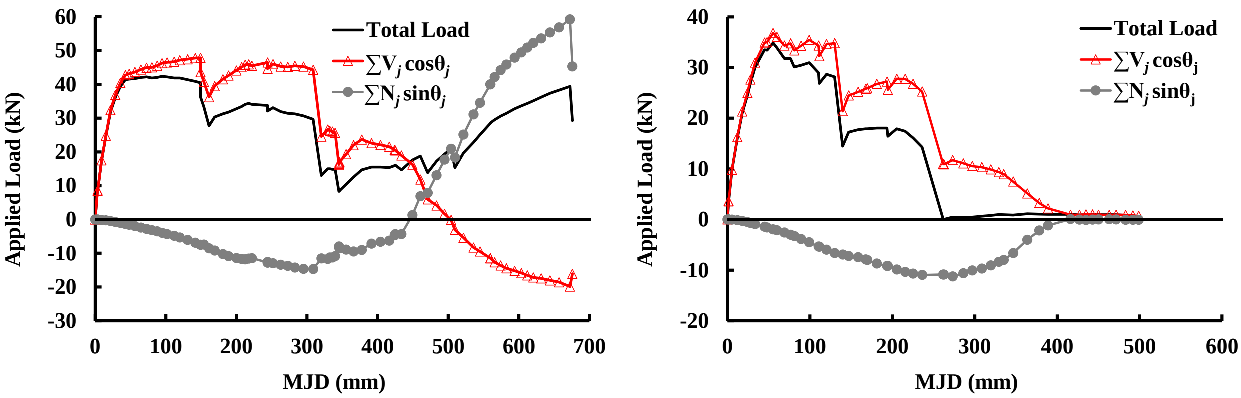

(a)

(b)

Fig. 19. De-composition of the vertical resistance: (a) RC-Con; (b) PC-EP

Conflict of interest

The authors declare that there is no conflict of interest regarding the publication of this paper.

Corresponding Author: Yun-Hao Weng, wengyh@st.gxu.edu.cn

Author Statements

Xiao-Fang Deng: Supervision. **Teng-Fang Dong:** Methodology and Formal Analysis. **Feng Fu**: Resources. **Yun-Hao Weng:** Writing-Original Draft Preparation.

Resilience of Prefabricated Concrete Frames using Hybrid Steel-Concrete Composite Connections

Xiao-Fang Deng[1], Teng-Fang Dong[1], Feng Fu[1,2], and Yun-Hao Weng[1*]

[1] College of Civil Engineering and Architecture, Guilin University of Technology, Guilin, China, 541004.

[2] School of Mathematics, Computer Science and Engineering, City, University of London, EC1V0HB, UK.

Abstract:

The progressive collapse resistance of prefabricated concrete frames with hybrid steel-concrete composite connections (HSCC) is rarely studied. To fill the gap, five (one reinforced concrete (RC) and four prefabricated concrete) 1/2 scaled beam-column sub-assemblages were designed and tested. In four prefabricated concrete specimens, different HSCC types, top and seat with web angle (TSWA), end plate (EP), top and seat angle (TSA), and web cleat (WC), were employed. Experimental results demonstrated that the failure patterns of prefabricated concrete frames with HSCC are different from that of the RC frame counterpart. The failure of the prefabricated concrete frames is governed by the shear fracture or thread stripping of the bolts in the connections while that of the RC frame is governed by the fracture of beam longitudinal rebar. Due to brittle failure of the connections in prefabricated concrete frames, both ultimate bearing capacity and deformation capacity of prefabricated concrete frames are smaller than the corresponding RC frame. Among them, the prefabricated concrete frame with the EP connection achieves the greatest first peak load or compressive arch action capacity. However, no catenary action could be developed in this specimen.

Author Keywords: Disproportionate collapse; Hybrid prefabricated concrete frame; Load resisting mechanism; Beam-column sub-assemblage; Experimental results

* Corresponding author, E-mail address: wengyh@st.gxu.edu.cn

1. Introduction

According to the ASCE/SEI-10 [1], disproportionate collapse is defined as "the spread of an initial local failure from element to element eventually leading to the collapse of an entire structure or a disproportionately large part of it." In recent years, with the frequent occurrence of extreme events, such as terrorist attacks, fires, and explosions, the likelihood of disproportionate collapse caused by extreme loads was increasing. The disproportionate collapse of structure usually results in substantial economic and life loss. How to evaluate or enhance the ability of structures to resist disproportionate collapse has attracted increasing attention from engineers and policymakers. Several design guidelines [1-4] were issued successively. The alternative load path (ALP) method was proposed and gradually became the most popular method in design or academic investigations as it was independent of the extreme loading [5]. Based on the ALP method, many studies were conducted in the past decades [6-9]. Structures may lose columns after an accidental event, causing a significant increase in shear force and flexural bending moment of the adjacent structural components. The beams adjacent to the lost columns can't resist such a significant amount of bending moment purely relying on their flexural strength. Therefore, exploring the inherent potential mechanisms is necessary. The inherent mechanisms include catenary action (CA) and compressive arch action (CAA) of the beams, and tensile membrane action (TMA) and compressive membrane action (CMA) of the slabs.

With the development of modular building technologies, prefabricated concrete (PC) structures have been widely used in developed countries. Several studies [10-15] were carried out to investigate the disproportionate collapse resistance of conventional PC structures with dry or wet connections. Moreover, as steel-concrete composite joints offer an efficient method to connect precast columns and beams, various hybrid steel-concrete composite (HSCC) structures were developed. Compared to the conventional connection of prefabricated concrete structures, the use of hybrid steel-concrete composite (HSCC) connections offers advantages of both steel and concrete materials. It is possible to reduce the size of both hybrid precast beams and columns through effective interaction between the two materials. Moreover, the HSCC connections can be connected by using high-strength bolts or welds, which required less on-site work. Thus, the HSCC structure is ideal for PC buildings [16]. In the past decades, the seismic behavior of PC frames with various types of HSCC connections was investigated. Kulkarni et al. [17] and Li et al. [18] conducted experimental and analytical investigations on HSCC connections subjected to quasi-static cyclic loading to reveal their seismic behavior. It was found that the HSCC connections exhibited sufficient ductility under seismic loading. Li et al. [19] tested a new-type of HSCC connection with end plates to investigate its seismic behavior. It was revealed that the HSCC connection performed even better than the conventional RC connection. Zhang et al. [20] developed a new type of HSCC connection using steel fiber concrete. It was found that the proposed HSCC connection had a satisfactory ability to resist seismic loads. In addition, Zhang et al. [21] designed an innovative type of HSCC connection with energy dissipated plates and I-shaped steel connectors. It revealed that the hybrid joints with the energy dissipated plates and steel fiber concrete performed much better.

From the above investigations, it can be seen that the HSCC connection has been proved to be an effective type of connection for PC frames to resist seismic loadings. However, the characteristics of disproportionate collapse are quite different from those of a seismic hazard: such as the loading direction, monotonic or cyclic, the main load resisting components, etc. Moreover, the resilience of PC frames with HSCC connection to resist disproportionate collapse was still unclear due to few available studies. Therefore, to fill this gap, four PC beam-column assemblies with HSCC connections and one counterpart sub-assemblage using normal RC were designed and tested in this study. The difference between PC frames with HSCC connections and RC frame in terms of load resisting mechanisms were quantified and discussed.

2. Experimental program

2.1. Specimen design

To investigate the resilience of PC frames with HSCC connections, five 1/2 scaled beam-column assemblies were fabricated and tested. Among them, four PC beam-column s assemblies were designed with various HSCC connections and the remaining one is a cast-in-place RC sub-assemblage, which was taken as a control specimen for comparison. The prototype frame of the specimen is a 5-story commercial building that is seismically designed by BS 8110-97 [22], following Kulkarni et al. [17]. Both longitudinal and transverse spans of the prototype frame are 6 m. The story height is 4.1 m. It was assumed that a middle column on the ground floor was lost due to extreme loading. The sub-assemblage above the lost column was extracted from the prototype frame for the test. Therefore, all specimens consist of a two-span beam, a short middle column stub, two side columns, and two overhanging beams, as shown in Fig. 1. The height of the side column and the length of the overhanging beam is determined by the position of inflection points. It was assumed that the inflection points were in the middle height of the column and 1/5 span of the beam. The cast-in-place RC specimen was named as RC-Con, and its dimensions and rebar details are illustrated in Fig. 2. As can be seen in the figure, the clear span of the beam is 2750 mm. The cross-section of the beam and column is 150 mm × 250 mm and 250 mm × 250 mm, respectively. In this study, a relatively low reinforcement ratio is used to make the effect of CAA obvious. T10 and T13 are used as longitudinal rebar while R6 is used as transverse rebar. The beam transverse rebar in the potential plastic hinge zone and the remaining zones were R6@70mm and R6@140mm, respectively, to follow the seismic design details. “T” and “R” represent deformed rebar and plain rebar, respectively. Detailed specimen properties of RC-Con were shown in Table 1.

For PC specimens, four different bolted connections were investigated. Based on the connection types, the specimens were named as follows: PC specimen with TSWA connection was named as PC-TSWA, PC specimen with end plate connection was named as PC-EP, PC specimen with top and seat angle connection was named as PC-TSA, and PC specimen with web cleat connection was named as PC-WC. As shown in Fig. 3, except for the beam-column connection, the dimensions and rebar details of the PC specimens are identical to those of the control specimen RC-Con. The detailing of different HSCC connections is shown in Fig. 4 and tabulated in Table 2, and the detailed fabrication process was illustrated in Fig. 5. For PC-TSWA, the PC beam and column were connected by top and seat angles with double web angles. The angles were connected to the PC beams and columns using M10 size bolts. In terms of PC-EP, the PC beam was connected to the PC column by an end plate. The end plate was welded to the PC beam, and six M10 bolts were applied to fasten the end plate to the PC column. Only top and seat angles were used to connect the PC beam and column in PC-TSA, and only double web angles were applied to connect the PC beam and column in PC-WC. It should be noted that the connectors of PC beams and columns were made of I-shaped steels with the section of UB178×101×19 and UC 203×203×46, respectively. The length of I-shaped steel in the PC beam is 125 mm and that in the PC column is 710 mm. The strength grade of the I-shaped steel is S355. The longitudinal rebar of the PC beams and columns are welded to the I-shaped connectors. For PC-TSWA, PC-TSA, and PC-WC, steel angles with a section size of L60×6 mm were used. For PC-EP, the end plates were 160×220×10 mm and were welded to the I-shaped connectors in PC columns.

2.2. *Property of materials*

According to the compressive and tensile splitting cylinder tests, the average compression strength and splitting tensile strength of the concrete are 34 MPa and 3.3 MPa, respectively. The critical properties of rebar and steel angles are listed in Table 3.

2.3. Test setup with instrumentation layout

In this study, a displacement-controlled pushdown loading regime was applied. The test setup and instrumentation layout are displayed in Fig. 6. This setup was commonly used for pushdown tests of disproportionate collapse resilience of structures [23-27]. As mentioned above, the specimens were extracted from the prototype frame at contraflexure points and 1/2 scaled down. Thus, the side column was pin supported with a roller installed horizontally at the top of the side column and overhanging beam end to represent the horizontal restraints from adjacent members. An axial force of $0.2f_c^{'}A_g$ (where $f_c^{'}$ is the cylinder compressive strength of concrete while A_g is the gross area) was applied on the side column. To assess the bridging capacity of the specimen under the loss of a middle column, a vertical displacement with the rate of 0.2mm/s was applied to the top of the middle column by a jack with a 700 mm stroke (Item 1 in Fig. 6). A specially designed steel assembly (Item 3 in Fig. 6) was installed for preventing the undesired out-of-plane failure.

A series of load cells, displacement transducers, and strain gauges were applied before testing. Load pins (Item 6 in Fig. 6) were applied in the pin supports to measure the reaction forces of pin support. Tensile/compressive both way load cell (Item 5 in Fig. 6) was applied in each horizontal roller to record its horizontal reaction force. During testing, the applied vertical load was measured by a load cell (Item 2 in Fig. 6) installed between the hydraulic jack (Item 1 in Fig. 6) and the reaction frame. Seven displacement transducers (Item 7 and 8 in Fig. 6) were applied along the beam span to record beam deflection shape. In addition, a series of strain gauges were glued on the rebar at special positions before casting, as shown in Figs. 2 and 3.

3. Test results

In the present study, one RC and four PC beam-column assemblies were tested by pushdown loading regime to assess the effects of different HSCC connections on the performance of PC frames to resist disproportionate collapse. The key results of the test were listed in Table 4 and discussed below.

3.1 Global behavior

3.1.1 Specimen RC-Con

Specimen RC-Con is the cast-in-place RC beam-column sub-assemblage. The load-middle joint deflection (MJD) relationship and failure pattern of RC-Con are displayed in Figs. 7 and 8, respectively.

Initially, the first crack formed at the beam near the middle column at the MJD of 12 mm. With the MJD further increasing to 15 mm, the RC-Con reached its first yield load (FYL), which was defined as the vertical load corresponding to the first yield of the beam longitudinal rebar, of 25 kN. The actual moment applied at the beam ends near the middle column was 16 kN·m, which is 64% of the maximum moment resisted at the section. Meanwhile, noticeable cracks were formed near the beam ends. When the MJD reached 73 mm, the first peak load (FPL) of 42 kN was measured, which is 168 % of FYL, indicating that the load capacity is increased by 68 % due to the mobilization of CAA. The ratio of the actual moment applied to the maximum moment resisted at the beam ends near the middle column increased to 97 % at this time. When MJD reached 120 mm, the actual moment applied at the beam ends near the middle column attained its maximum. With a further increase in MJD, the existing cracks became wider, and the load resistance began to decrease due to the concrete crushing. Further increasing MJD to 154 mm, fracture was occurred in the rebar near the middle column, resulting in the load resistance dropping to 28 kN. Meanwhile, the widest cracks appeared at the location of curtailment of the beam longitudinal rebar. When MJD reached 309 mm, rebar fracture was also observed in the curtailment region of the longitudinal rebar, leading to a further decrease in the load resistance. Once MJD exceeds 448 mm, the load resistance enhanced rapidly since the development of CA. Finally, the ultimate load capacity (UL) of 39 kN was recorded at the MJD of 672 mm. As displayed in Fig. 8, rebar fracture appeared in the beam ends near the middle column and cut-off points of the longitudinal rebar. Obvious concrete crushing occurred in the beam ends. Many penetrated cracks were formed along the beams due to tensile axial force developed in the CA stage.

3.1.2 Specimen PC-TSWA

Specimen PC-TSWA is a PC beam-column sub-assemblage with HSCC of TSWA connection. The vertical load-MJD relationship and failure pattern are displayed in Figs. 7 and 9. Similar to RC-Con, at the MJD of 10 mm, crack first formed at the beam ends near the middle column. When MJD obtained 38 mm, the FYL was measured at 25 kN. The ratio of the actual moment applied to the maximum moment resisted at the beam ends near the middle column reached 65 %. Further growing MJD to 132 mm, the specimen reached FPL of 33 kN, which is 132 % of FYL, indicating that the load capacity is increased by 32 % because of the mobilization of CAA. At this time, the ratio of the actual moment applied to the maximum moment resisted at the beam ends near the middle column increased to 99%. Then, with the increase of MJD, the load resistance of the specimen decreased slowly due to concrete crushing occurred. Meanwhile, large openings were observed at the edge of the I-shaped connectors near the middle column. The applied moment reached its maximum at MJD of 149 mm. When MJD reached 152 mm and 166 mm, the beam rebar fractured at the edge of the I-shaped connectors near the middle column. When the MJD exceeded 229 mm, the bolts at the top angle near the side column were sheared off. Then, the bolts at the web angle began to be sheared off at the MJD of 326 mm. The CA began to develop at the MJD of 385 mm. Finally, following the shear fracture of the bolts at the bottom angle near the side column, PC-TSWA reached its UL of 19 kN, which was only 58 % of its FPL. As displayed in Fig. 9, rebar fracture occurred at the edge of the I-shaped connectors near the middle column. The failure at the side connection was controlled by bolt fracture in shear. Concrete crushing was observed in the beam ends near the middle column while concrete shed occurred in the beam ends near the side column. The number of flexural cracks was much less than those in RC-Con.

3.1.3 Specimen PC-EP

PC-EP is a PC beam-column sub-assemblage with HSCC of end plate connection. The vertical load-MJD relationship and failure pattern are shown in Figs. 7 and 10, respectively. Different from RC-Con and PC-TSWA, the first crack of PC-EP occurred at the edge of the I-shaped connectors near the middle column at the MJD of 12 mm. When MJD increased to 18 mm, the specimen reached its FYL of 21 kN. The ratio of the actual moment applied to the maximum moment resisted at the beam ends near the middle column reached 48 %. Further increasing the MJD to 55 mm, the FPL of 35 kN, which is 167 % of FYL, was measured. This indicated that the mobilization of CAA increases the load capacity by 67 %. At this time, the ratio of the actual moment applied to the maximum moment resisted at the beam ends near the middle column increased to 95%. Then, with the increase of MJD, thread stripping of the bolt occurred at the connections near the side column, leading to the decrease in load resistance. When the MJD reached 130 mm, the applied moment reached its maximum. At the MJD of 236 mm, the load resistance dropped to zero due to bottom rebar fracture. Finally, further increasing the MJD, as the side connections failed by thread stripping of all bolts, the beams and side columns were separated completely. Therefore, CA was not triggered and the load resistance held steady, which was only about 1 kN. As displayed in Fig. 10, rebar fracture occurred at the edge of the I-shaped connectors near the middle column. Moreover, the beam lost contact with the side column finally due to thread stripping of the bolts. Concrete crushing occurred at the edge of the I-shaped connectors near the middle column. The flexural cracks were much less than those in RC-Con and PC-TSWA. No penetrated cracks formed along the beam due to no CA mobilized during the test.

3.1.4 Specimen PC-TSA

PC-TSA is a PC beam-column sub-assemblage with HSCC of top and seat angle connection. The vertical load-MJD relationship and failure pattern are shown in Figs. 7 and 11, respectively. Similar to RC-Con and PC-TSWA, the first crack of PC-TSA occurred at the beam with the MJD of 8 mm. As the beam longitudinal rebar did not yield before FPL, no FYL is shown herein. The FPL of 20 kN was obtained at the MJD of 87 mm. The ratio of the actual moment applied to the maximum moment resisted at the beam ends near the middle column was 83% at this time. Then, further increasing MJD, the load resistance decreased slowly due to concrete crushing. When MJD reached 204 mm and 261 mm, the angle bolts fractured in shear, leading to the load resistance dropping to 0 kN rapidly. The maximum moment of the beam ends near the middle column was measured at the MJD of 204 mm.

Then, with the increase of MJD, the load resistance increased again. Finally, when MJD reached 432 mm, PC-TSA failed by the shear damage of the bolts and achieved its UL of 10 kN. As shown in Fig. 11, all connections failed by bolt shear fracture. Concrete crushing and spalling appeared in the beam ends. Similar to PC-EP, no penetrated cracks formed in the middle zones of the beam due to mild CA developed.

3.1.5 Specimen PC-WC

PC-WC is a PC beam-column sub-assemblage with HSCC of web cleat connection. The vertical load-MJD relationship and failure pattern are shown in Figs. 7 and 12. The first crack was measured at beam ends at the MJD of 7 mm. Similar to PC-TSA, there was no FYL because no beam longitudinal rebar yielded before FPL. When MJD reached 109 mm, the specimen obtained its FPL of 19 kN. The applied moment at the beam ends near the middle column was 14 kN·m, which is 77% of the maximum moment. Then, the load resistance started to drop slowly accompanied by the concrete crushing and spalling. After the MJD exceed 230 mm, the bolts began to fracture due to shear force. The maximum moment of the beam ends near the middle column was measured at the MJD of 299 mm. Finally, as all bolts of the connection near the middle column were destroyed completely at the MJD of 436 mm, the specimen reached its UL of 12 kN. As shown in Fig. 12, the failure of connections was caused by the shear fracture of bolts. Concrete spalling occurred at beam ends. Similar to PC-EP, PC-TSA, no penetrated cracks occurred in the middle zones of the beam since less tensile axial force developed in the beams.

3.2 Horizontal reactions

As the specimens' arrangements were all symmetrical, the average value of the horizontal reaction forces obtained at both sides of the specimens was used and discussed. The horizontal reaction force-MJD curves of the specimens are displayed in Fig. 13. The maximum horizontal reaction forces of the specimens were tabulated in Table 4. Negative means compression force while positive represents tension force. As given in Fig. 13(c), no tensile horizontal force was measured in PC-EP, which confirmed the above conclusion that no CA was developed in the beams due to complete tread stripping of the bolts at MJD of 337 mm. Different from PC-EP, both tensile and compressive reaction forces were measured in other specimens. The maximum horizontal compression forces of RC-Con, PC-TSWA, PC-EP, PC-TSA, and PC-WC are -71 kN, -65 kN, -67 kN, -56 kN, and -56 kN. The maximum horizontal tension forces of RC-Con, PC-TSWA, PC-TSA, and PC-WC were 95 kN, 47 kN, 20 kN, and 24 kN. Therefore, the CAA and CA developed in PC frames with HSCC connection were weaker than those in RC-Con. Among the PC specimens, PC-EP achieved a similar compressive reaction force as that of PC-TSWA. PC-TSA and PC-WC achieved similar horizontal reaction forces.

As shown in Fig. 13, for all specimens, in the stage of CAA, the compressive reaction force was primarily from the bottom pin support. In the large deformation stage, the tensile reaction force of RC-Con was mainly provided by the horizontal restraint at overhanging beam. However, for PC specimens, the tensile reaction force was mostly from the top horizontal restraint and bottom pin support. This is because, in the large deformation stage, the development of axial force in beams of PC specimens is hindered due to the shear fracture of bolts. Therefore, for PC specimens, the shear forces of the side columns transferred from the beams are small, resulting in a small lateral deformation of the side column. Thus, a relatively small force is transmitted to the horizontal restraint at the overhanging beam.

3.3 Deformation's shape

The deformation's shape of the beams is monitored by LVDTs along the beam. Fig. 14 displays the deformation's shape of the beams of RC-Con and PC-TSWA at critical status. The dashed straight line represented chord rotation. As specified in DoD [4], it is calculated by the ratio of MJD to the clean beam span. As shown in Fig. 14(a), for RC-Con, the beams kept almost straight before the FPL. With the MJD increasing to 250 mm, the rotation of the beam end near the middle column was greater than that near the side column. In the last stage, the chord rotation overestimates the rotation of the beam end near the side column and underestimates the rotation of the beam end near the middle column. This is because the plastic hinge formed at the curtailment of the beam longitudinal rebar. Different from RC-Con, as displayed in Fig. 14(b), the beams in PC-TSWA kept straight during the whole loading history. At the UL stage, the chord rotation could predict the rotation of the beam end near the side column accurately but overestimated the rotation of the beam end near the middle column due to plastic hinges occurring at the edge of the I-shaped connectors. For PC-TSA and PC-WC, the rotation of the beam ends was consistent with the chord rotation well. For PC-EP, the deformation of the beam was similar to that of PC-TSWA.

3.4 Strain gauge results

The location of strain gauges is shown in Figs. 2 and 3. The bottom longitudinal rebar of RC-Con, PC-TSWA, and PC-EP started to yield at the MJD of 15 mm, 38 mm, and 18 mm. However, no yielding was measured in PC-TSA during the whole test history while yielding strain was only measured at PC-WC until the stage of UL. Figs. 15 to 16 show the strain readings along with longitudinal rebar of PC-TSWA, and PC-EP, respectively. For PC-TSWA, after reaching FPL, the compression strain of the rebar near the middle column began to decrease with the increase of MJD, indicating that the CAA stage was shifted into the CA stage. However, beyond the stage of FPL, the decrease in load resistance of PC-EP was due to bolt thread stripping instead of concrete crushing. Therefore, different from other specimens, the compression strain of the rebar near the middle column of PC-EP continued to increase after the stage of FPL, which can be seen in Fig. 16. In addition, for PC-TSWA, in the large deformation stage (UL or MJD = 500 mm), most of the longitudinal rebar was in tension, which indicates that CA could have developed in these specimens. Conversely, most of the longitudinal rebar strains of PC-EP were very low in the large deformation stage, indicating that no CA was developed, which is consistent with the results of vertical loads and horizontal reactions. The development of the rebar strain of RC-con, PC-TSA, and PC-WC is similar to PC-TSWA.

4. Analytical and discussion

4.1 Effects of HSCC connection types

As shown in Table 4, the FPL of PC-TSWA, PC-EP, PC-TSA, and PC-WC is 79 %, 83 %, 48 %, and 45 % of that of RC-Con, respectively. Thus, the PC frames using the proposed four HSCC connections could not achieve equivalent behavior as cast-in-place RC frames regarding FPL. Moreover, the measured deformation capacity of RC-Con, PC-TSWA, PC-TSA, and PC-WC corresponding to their UL is 672 mm, 413 mm, 236 mm, 432 mm, and 436 mm, respectively. Therefore, the deformation capacity of PC-TSWA, PC-EP, PC-TSA, and PC-WC is 61 %, 35 %, 64 %, and 65 % of that of RC-Con, respectively. Furthermore, the UL of PC-TSWA, PC-EP, PC-TSA, and PC-WC is 49 %, 36 %, 26 %, and 31 % of that of RC-Con, respectively. It should be noted that the UL is defined as the peak load in the re-ascending phase of the load history. Therefore, regarding the deformation capacity and UL, the PC frames with the proposed four HSCC connections still could not be equivalent to the cast-in-place frame. The lower FPL is due to the lower strength of the HSCC connection and weaker CAA. On the other hand, the lower deformation capacity is because the failure patterns of all PC specimens are controlled by shear fracture or thread stripping failure of the bolts, which are brittle failures and thus, reduce the ductility of the specimens. In consideration that the failure patterns of PC specimens may be changed if the greater size bolts or weaker steel plates are designed in HSCC connection. Therefore, more studies are urgently in need to further investigate the robustness of PC frames with HSCC connections to resist disproportionate collapse in the future.

For PC specimens, the FPL of PC-EP is larger than that of PC-TSWA. However, due to thread stripping failure at the MJD of 337 mm, which prevents the development of CA and thus, the deformation capacity and UL of PC-EP is much lower than that of PC-TSWA.

4.2 Dynamic ultimate bearing capacity

It should be noted that disproportionate collapse is generally a dynamic process. Therefore, it is needed to assess their dynamic ultimate bearing capacity. Relied on the quasi-static pushdown load-displacement curve, a capacity curve method [28] was adopted to calculate the dynamic ultimate bearing capacity of the specimens. Previous studies [29] had been confirmed the feasibility of this method. The mathematical equation of the capacity curve method is given in Eq. 1:

$$P_d\left(u_d\right)=\frac{1}{u_d}\int_0^{u_d} P_s\left(u\right)d_u \tag{1}$$

where $P_d\left(u_d\right)$ and $P_s\left(u\right)$ represent the capacity function and the nonlinear static loading estimated at the displacement demand u, respectively.

Fig. 17 compares the dynamic load-MJD curves of the test specimens based on the capacity curve method. As displayed in the figure, the dynamic ultimate bearing capacity of PC-TSWA, PC-EP, PC-TSA, and PC-WC is 71 %, 73 %, 47 %, and 42 % of that of RC-Con, respectively. Thus, the quasi-static pushdown curve is a good alternate method for the disproportionate collapse study. The dynamic load increase factor is defined as the ratio of static ultimate bearing capacity to dynamic load-resisting capacity [27]. Based on the test results and analytical results, the dynamic load increase factors of RC-Con, PC-TSWA, PC-EP, PC-TSA, and PC-WC were 1.11, 1.22, 1.25, 1.11, and 1.19. Among them, the dynamic load increase factor of the PC specimens is greater than that of the RC specimen due to the brittle failure that occurred there.

4.3 Effects of steel angles

As shown in Table 4 and Fig. 7, the FPL of PC-TSWA is 165 % and 174 % of that of PC-TSA and PC-WC, respectively. Therefore, the web angles and top and seat angles increase the FPL by 65 % and 74 %, respectively. For UL, PC-TSWA, PC-TSA, and PC-WC are 19 kN, 10 kN, and 12 kN. The corresponding MJD is 413 mm, 432 mm, and 436 mm. The results show that the additional web angle or top and seat angle has little effect on the deformation capacity. However, the web angle and top and seat angle could increase the UL by 90 % and 58 %, respectively. Analytical results indicated that the web angle and top and seat angle enhanced the dynamic ultimate bearing capacity by 50 % and 69 %.

4.4 De-composition of vertical load resistance

According to the force equilibrium of the deformed beam in Fig. 18, the vertical load resistance at the middle column could be divided into:

$$P = \sum_{j=1}^{2}\left(N_j \sin\theta_j + V_j \cos\theta_j\right) \tag{2}$$

where *P*= the applied load; N_j and V_j = the axial force and shear force; θ_j =the rotation of the beam section at one of the joint interfaces.

Based on Eq. (2), the contribution of the axial force (related to CA) and shear force (related to flexural action) could be calculated. The de-composition of load resistance is shown in Fig. 19. PC-TSWA, PC-TSA, and PC-WC have a similar response as RC-Con in terms of de-composition of load resistance. Before CA is triggered, the contribution of axial force is negative, and the vertical load was mainly provided by the flexural action. After the fracture of the rebars or bolts, the contribution of flexural action dropped significantly. In the CA stage, the contribution of CA is positive, while the contribution of flexural action kept decreasing. When the bottom rebar or bolts of the connection near the middle column fractured entirely, the contribution of flexural action transferred into negative. For PC-EP, as no CA developed, the vertical load is mainly provided by the flexural action while the contribution of CA is positive during the test.

5. Conclusions

To examine the resilience of PC frames using innovative hybrid steel-concrete composite (HSCC) connections to resist disproportionate collapse, a series of four PC beam-column assemblies with various HSCC connections as well as an RC sub-assemblage were tested in this study. Relied on the experimental and analytical results, the main conclusions were given:

1. The failure pattern of PC frames with HSCC connections is different from RC frames. The failure of PC frames with HSCC connection is mainly controlled by the shear failure or thread stripping of the bolts. However, the failure of the RC frame is normally controlled by the fracture of top

longitudinal rebar at cut-off points or bottom longitudinal rebar at beam ends near the middle column. Moreover, the beams in PC frames with HSCC connections kept straight during the test, which means rotation mainly concentrated into the HSCC connection.

2. RC frame has larger FPL and UL than those of PC frames with HSCC. Together with horizontal reaction force results, considerable CAA and catenary action capacity are only measured in PC-TSWA. Almost no catenary action is mobilized in the remaining PC frames with EP, TSA, or WC connections. Thus, the load resisting mechanism of PC frames with HSCC is highly dependent on the type of HSCC connection and different from that in RC frames.
3. Comparing the results of PC-TSWA, PC-TSA, and PC-WC, the web angles and top and seat angles enhanced the first peak load of PC frames by 65 % and 74 %, respectively. In addition, the additional web angles or top and seat angles have little effect on the deformation capacity, but could increase the UL by 90 % and 58 %.
4. De-composition of the vertical load resistance indicated that the load contribution in PC-TSWA, PC-TSA, PC-WC, and RC-Con is similar. In the small deformation stage, the vertical load mainly comes from flexural action. Nevertheless, the vertical load is mainly from the development of catenary action in the large deformation stage. However, for PC-EP, the vertical load is mainly from the flexural action during the test.

Acknowledgements

The authors gratefully acknowledge the financial support provided by the National Natural Science Foundation of China (No. 52022024) and the Natural Science Foundation of Guangxi (No. 2021GXNSFFA196001). Any opinions, findings, and conclusions expressed in this paper do not necessarily reflect the view of the National Natural Science Foundation of China and the Natural Science Foundation of Guangxi.

References

[1] ASCE/SEI, Minimum design loads for buildings and other structures, ASCE/SEI 7, Reston, VA, 424, 2010.
[2] General Services Administration (GSA), Progressive collapse analysis and design guidelines for new federal office buildings and major modernization projects, Washington, DC, 2003.
[3] European Committee for Standardization (CEN), Eurocode 1: Actions on structures. Part 1-7: General actions-Accidental actions, EN 1991-2-7, Brussels, 2006.
[4] Department of Defense (DoD), Design of buildings to resist progressive collapse, Unified Facilities Criteria (UFC) 4-023-03, Washington, DC, 2013.
[5] B.R. Ellingwood, D.O. Dusenberry, Building design for abnormal loads and progressive collapse, Comput.-Aided Civ. Infrastruct. Eng. 20(3) (2005) 194-205.
[6] F. Sadek, J.A. Main, H.S. Lew, Y.H. Bao, Testing and analysis of steel and concrete beam-column assemblies under a column removal scenario, J. Struct. Eng. 137(9) (2011) 881-892.
[7] H. Choi, J. Kim, Progressive collapse-resisting capacity of RC beam-column sub-assemblage, Mag. Concr. Res. 63(4) (2011) 297-310.
[8] J. Yu, K.H. Tan, Special detailing techniques to improve structural resistance against progressive collapse, J. Struct. Eng. 140(3) (2014) 04013077.
[9] K. Qian, B. Li, J. Ma, Load-carrying mechanism to resist progressive collapse of RC buildings, J. Struct. Eng. 141(2) (2015) 04014107.
[10] S.B. Kang, K.H. Tan, Robustness assessment of exterior precast concrete frames under column removal scenarios, J. Struct. Eng. 142(12) (2016) 04016131.
[11] S.B. Kang, K.H. Tan, Progressive collapse resistance of precast concrete frames with discontinuous reinforcement in the joint, J. Struct. Eng. 143(9) (2017) 04017090.
[12] K. Qian, B. Li, Performance of precast concrete substructures with dry connections to resist progressive collapse, J. Perform. Constr. Facil. 32(2) (2018) 04018005-1-14.
[13] D.C. Feng, G. Wu, Y. Lu, Numerical investigation on the progressive collapse behavior of precast reinforced concrete frame subassemblages, J. Perform. Constr. Facil. 32(3) (2018) 04018027.
[14] Y. Zhou, T. Chen, Y. Pei, H.J. Hwang, X. Hu, W. Yi, L. Deng, Static load test on progressive collapse resistance of fully assembled precast concrete frame structure, Eng. Struct. 200 (2019) 109719.
[15] Y. Zhou, X. Hu, Y. Pei, H.J. Hwang, L. Deng, Dynamic load test on progressive collapse resistance of fully assembled precast concrete frame structures, Eng. Struct. 214 (2020) 110675.

[16] S.C. Park, W.K. Hong, S. Kim, X. Wang, Mathematical model of hybrid precast gravity frames for smart construction and engineering, Math. Probl. Eng. 2014 (2014) 1-14.

[17] S.A. Kulkarni, B. Li, W.K. Yip, Finite element analysis of precast hybrid-steel concrete connections under cyclic loading, Steel Const. 64(2) (2008) 190-201.

[18] B. Li, S.A. Kulkarni, C.L. Leong, Seismic performance of precast hybrid-steel concrete connections, J. Earthq. Eng. 13(5) (2009) 667-689.

[19] S. Li, Q. Li, H. Zhang, H. Jiang, L. Yan, W. Jiang, Experimental study of a fabricated confined concrete beam-to-column connection with end-plates, Constr. Build. Mater. 158 (2018) 208-16.

[20] J. Zhang, C. Ding, X. Rong, H. Yang, K. Wang, B. Zhang, Experimental seismic study of precast hybrid SFC/RC beam-column connections with different connection details, Eng. Struct. 208 (2020) 110295.

[21] J. Zhang, C. Ding, X. Rong, H. Yang, Y. Li, Development and experimental investigation of hybrid precast concrete beam-column joints, Eng. Struct. 219 (2020) 110922.

[22] British Standards Institution (BSI), Structural use of concrete: Part 1: Code of practice for design and construction, BS 8110, Milton Keynes, UK, 1997.

[23] J. Yu, K.H. Tan, Structural behavior of reinforced concrete frames subjected to progressive collapse, ACI Struct. J. 114(1) (2017) 63-74.

[24] K. Qian, S.L. Liang, D.C. Feng, F. Fu, G. Wu, Experimental and numerical investigation on progressive collapse resistance of post-tensioned precast concrete beam-column sub-assemblages, J. Struct. Eng. 146(9) (2020) 04020170.

[25] Y.H. Weng, K. Qian, F. Fu, Q. Fang, Numerical investigation on load redistribution capacity of flat slab substructures to resist progressive collapse, J. Build. Eng. 29 (2020) 101109.

[26] K. Qian, S.Y. Geng, S.L. Liang, F. Fu, J. Yu, Effects of loading regimes on the structural behavior of RC beam-column sub-assemblages against disproportionate collapse, Eng. Struct. 251 (2022) 113470.

[27] K. Qian, S.L. Liang, X.Y. Xiong, F. Fu, Q. Fang, Quasi-static and dynamic behavior of precast concrete frames with high performance dry connections subjected to loss of a penultimate column scenario, Eng. Struct. 205 (2020) 110115.

[28] B.A. Izzuddin, A.G. Vlassis, A.Y. Elahazouli, D.A. Nethercot, Progressive collapse of multi-story buildings due to sudden column loss-Part 1: simplified assessment framework, Eng. Struct. 30(5) (2008) 1308-1318.

[29] K. Qian, B. Li, Research advances in design of structures to resist progressive collapse, J. Perform. Constr. Facil. 29(5) (2015) B4014007.